UNITED NATIONS EDUCATIONAL, SCIENTIFIC AND CULTURAL ORGANIZATION
INTERNATIONAL ATOMIC ENERGY AGENCY
INTERNATIONAL CENTRE FOR THEORETICAL PHYSICS
I.C.T.P., P.O. BOX 586, 34100 TRIESTE, ITALY, CABLE: CENTRATOM TRIESTE

H4.SMR/1011 - 28

Fourth Workshop on Non-Linear Dynamics and Earthquake Prediction

6 - 24 October 1997

Models of Dynamics of Seismicity

V.I. KEILIS-BOROK, A.A. SOLOVIEV et al

**International Institute of Earthquake Prediction
Theory and Mathematical Geophysics
Russian Academy of Sciences
Moscow, RUSSIAN FEDERATION**

NUMERICAL MODELLING OF BLOCK-STRUCTURE DYNAMICS BENEATH THE VRANCEA REGION

A. T. Ismail-Zadeh, V. I. Keilis-Borok, and A. A. Soloviev

International Institute of Earthquake Prediction Theory and Mathematical Geophysics, Russian Academy of Sciences, Warshavskoye sh. 79, kor. 2, Moscow 113556, Russia

Extended Abstract

This study is a first attempt to develop a numerical model of block structure dynamics (see Gabrielov et al., 1990 for a more detail) by using results of geodynamic modelling of mantle flows beneath a specific region. We apply this model to the earthquake-prone Vrancea region.

The Vrancea is situated at the bend of the Eastern Carpathians and controls the seismicity of Central and Eastern Europe. Gutenberg and Richter (1954) drew attention to the remarkable source of shocks with foci in the depth range 100 km to 150 km in Vrancea. The epicenters of mantle earthquakes in the Vrancea region are concentrated within a very small area (Fig.1, *a*). The projection of the foci on the NW--SE vertical plane AB across the bend of the Eastern Carpathians (Fig.1, *b*) shows a seismogenic body in the form of a parallelepiped with length of about 100 km, width of about 40 km, and extending to a depth of about 170 km. Beyond this depth no seismicity is observed.

It is suggested that the lithosphere is a hierarchical structure of blocks separated by fault zones (e.g., Alekseevskaya et al., 1977). In the model of block dynamics a seismic region is represented by a system of absolutely rigid blocks divided by infinitely thin plane faults. The blocks interact between themselves and with the surrounding medium. As the blocks are rigid, all deformation occurs in the fault zones and at interfaces separating the blocks and the surrounding medium. When the critical stress level (the upper stress threshold) is exceeded in some part of a fault plane, the

stress drops, possibly resulting in failures on other parts of the fault plane. The failures produce earthquakes. The parts of the fault plane where the failures have occurred are in a state of creep immediately after the earthquake for some time, while the stress remains below the low stress threshold. As a result of the numerical simulation a synthetic earthquake catalog is produced.

Panza et al. (1997) studied a model of block-structure dynamics of the Vrancea region where the block system moves due to prescribed horizontal motion of the boundary blocks. Ismail-Zadeh et al. (1996) and Ismail-Zadeh and Naimark (1997) developed a finite-element model of a slab sinking gravitationally in the mantle beneath the Vrancea region. They showed that the mantle flow induced by the sinking slab controls the shape of the slab, and the depth distribution of the annual average seismic energy released in earthquakes correlates with the depth distribution of stress in the slab.

In this study we develop a dynamical model of block structure through out the Vrancea lithosphere. The configuration of blocks and faults used in the model is presented in Fig.1, *c*. The values of the model parameters are shown in Table 1. The model structure contains eight faults. Fault 1 is an artificial one corresponding to the earth's surface; faults 2 and 8 are 'passive', because no shocks are observed there. The faults 1, 2, and 8 are immobile. The boundary faults 3, 4, 5, 6, and 7 move with prescribed velocities (V_X, V_Z) specified in Table 1. We prescribe the velocities using the numerical model of a sinking slab (Ismail-Zadeh et al., 1996). All deformations occur on these faults. We assume that the thickness of blocks is 100 km in this model. The magnitude of earthquakes is calculated by using the relationship $M = D \lg S + E$, where the constants D=0.98 and E=3.93 are given by Utsu and Seki (1954), and S is the sum of the squares of the cells involved in the earthquake.

The synthetic earthquake catalog is obtained as the result of block-structure dynamics simulation for a period of 300 units of dimensionless time. We study here the effect of slab rotation on the seismicity. To do it, we produce three synthetic catalogs for different values of angles of fault rotation ω (in 10^{-6} radians) around the origin of the

coordinates. Case 1. ω_i=0 on faults 4 (i=4), 5 (i=5), and 6 (i=6); case 2: ω_4=-0.0631, ω_5=-0.0571, and ω_6=-0.3225; case 3: the angles are increased by a factor of two (Table 1). The panels {Fig.1, *d-f*} show the distributions of focal depths contained in the synthetic catalog for these cases. The distribution of earthquake hypocenters in the synthetic catalog for case 1 (Fig.1, *d*) is in good agreement with that in the real catalog (Fig.1, *b*): the maximum value of magnitude, 7.1, in the synthetic catalog is close to that (M=7.2) observed in the region (Fuchs et al., 1979). Inspecting the panels, we conclude that small variations in the rotation angles result in changes of seismicity. Large synthetic earthquakes occur on faults 5 and 6 in case 1. The slab rotation tends to reduce earthquake magnitudes on fault 6 and to concentrate larger events on fault 5.

It follows that these changes in seismicity due to small variations in slab rotation are in overall agreement with the hypothesis of Press and Allen (1995), that small changes in the direction of plate motion control the pattern of seismic release. In the subsequent study we intend to verify this hypothesis on the basis of sophisticated block-structure models.

REFERENCES

Alekseevskaya, M. A., Gabrielov, A. M., Gvishiani, A. D., Gelfand, I. M. and Ranzman, E. Ya., 1977. Formal morphostructural zoning of mountain territories. J. Geophys., 43: 227-233.

Gabrielov, A.M., Levshina, T. A. and Rotwain, I. M., 1990. Block model of earthquake sequence. Phys. Earth Planet. Inter., 61: 18-28.

Ismail-Zadeh, A. T. and Naimark, B. M., 1997. Stress generation in sinking slabs beneath continental regions: Numerical models. Doklady Akademii Nauk, 354(4): 539-541.

Ismail-Zadeh, A. T., Panza, G. F. and Naimark, B. M., 1996. Stress in the descending relic slab beneath Vrancea, Romania, International Centre for Theoretical Physics. Internal Report IC/96/93, Trieste, Italy, 31 pp.

Panza, G. F., Soloviev, A. A. and Vorobieva, I. A., 1997. Numerical modelling of block-structure dynamics: Application to the Vrancea region. Pure Appl. Geophys., 149: 313-336.

Press, F. and Allen, C., 1995. Pattern of seismic release in the southern California region. J. Geophys. Res., 100: 6421-6430.

Utsu, T. and Seki, A., 1954. A relation between the area of aftershock region and the energy of main shock. J. Seismol. Soc. Japan, 7: 233-240.

TABLE 1. Model Parameters of Faults

Fault No.	Vertices of fault	V_x	V_z	ω		
				Case 1	Case 2	Case 3
1	1, 5, 2	0	0	0	0	0
2	2, 3	0	0	0	0	0
3	3, 4	0.199	0.065	0	0	0
4	5, 4, 6	4.726	-8.822	0	-0.063	-0.126
5	6, 7	1.817	-17.93	0	-0.057	-0.114
6	7, 8	5.635	-19.615	0	-0.322	-0.644
7	8, 9	-0.745	0.13	0	0	0
8	9, 1	0	0	0	0	0

Figure caption

Fig.1. Observed and modelled pattern of seismicity beneath the Vrancea region.

(a) Epicenters of Romanian earthquakes 1932 - 1996. Several real catalogs have been combined to prepare this and the next panels.

(b) Hypocenters of the same Romanian earthquakes (epicenters presented in panel a projected on the vertical plane AB along the NW-SE direction).

(c) The block structure used in numerical simulations; the numbers of vertices (*1-9*), faults (**1-8**}, and blocks (**I** and **II**) are indicated. The arrows stand for the velocities prescribed on boundary faults.

(d) -(f) Maps of synthetic seismicity for the region obtained by simulation of block-structure dynamics: case 1 (d), case 2 (e), and case 3 (f).

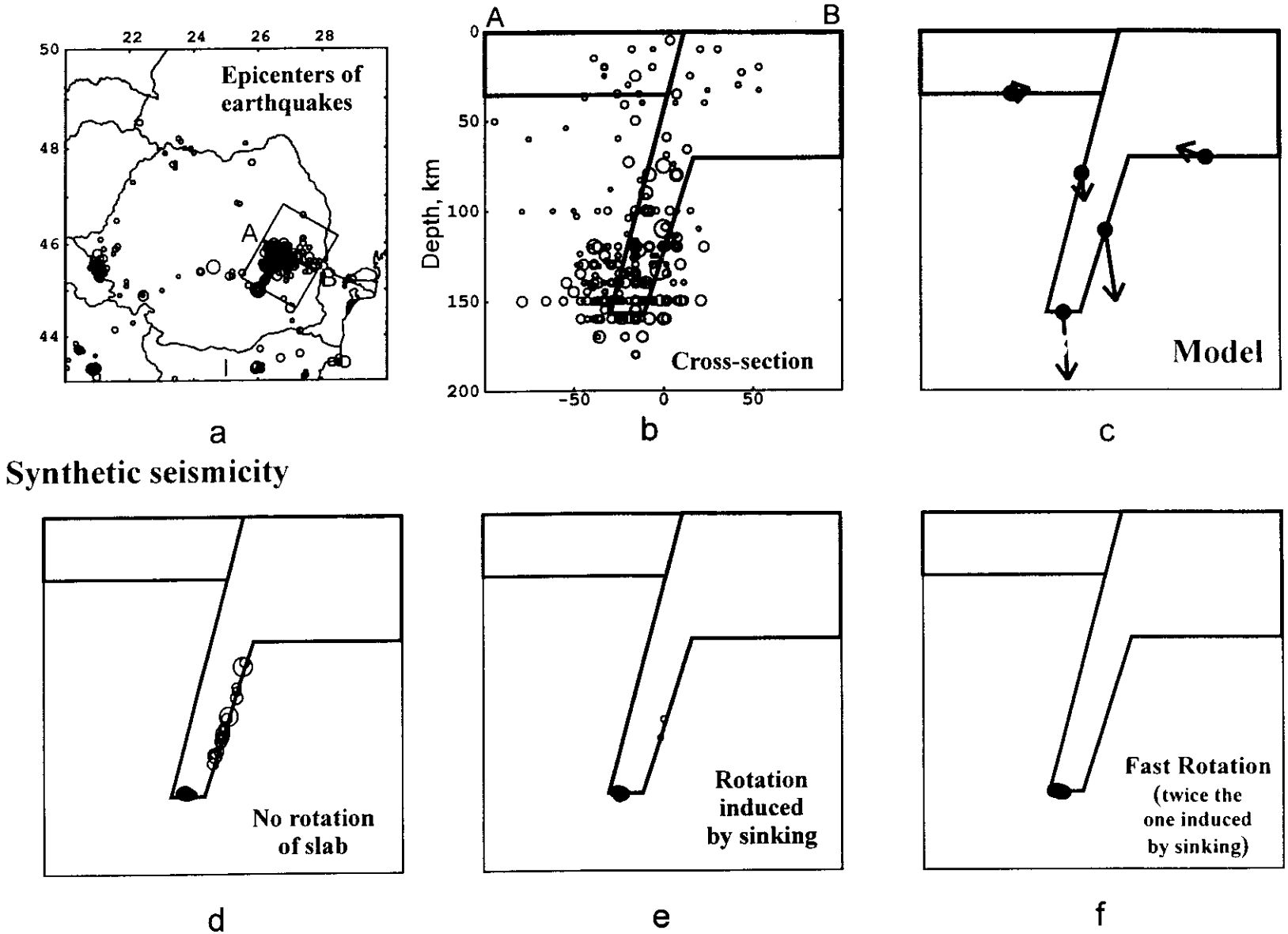

Fig.1. Observed and modelled pattern of seismicity beneath the Vrancea region.

(a) Epicenters of Romanian earthquakes 1932 - 1996. Several real catalogs have been combined to prepare this and the next panels.

(b) Hypocenters of the same Romanian earthquakes (epicenters presented in panel a projected on the vertical plane AB along the NW-SE direction).

(c)The block structure used in numerical simulations; the numbers of vertices (*1-9*), faults (**1-8**}, and blocks (**I** and **II**) are indicated. The arrows stand for the velocities prescribed on boundary faults.

(d)-(f) Maps of synthetic seismicity for the region obtained by simulation of block-structure dynamics: case 1 (d), case 2 (e), and case 3 (f).

M.G.Shnirman and E.M.Blanter

Self-Organized Criticality in a Mixed Hierarchical System

Self-organized criticality is obtained in a hierarchical system as a result of heterogeneity in the scaling conditions. A heterogeneous system consisting of a mixture of the simplest hierarchical models of failure is considered. Four kinds of model behavior are obtained: stability, catastrophe, unstable criticality and stable criticality (SOC). It is shown that the self-organized criticality is a characteristic of heterogeneity of medium. Possible applications of these results to earthquake prediction are discussed.

1. Introduction

Recently the self-organised criticality has been widely discussed because it is observed in numerous real systems of different nature [Bak et al, 1988]. In particular, it is a general property of the seismic process, regardless to concrete conditions in different seismic regions [Bak and Tang, 1989;Ito, 1992; Sornette and Sornette, 1989; Sornette et al, 1990].In opposite to unstable criticality appearing in isolated points of phase transition self-organised criticality exists in a wide interval of system parameters and may be referred to as a stable criticality. To understand the nature of this phenomenon it is important to extract conditions governing the appearance of self-organised criticality. Therefore investigations of simple models that exhibit self-organised criticality criticality would be very helpful [Bak and Tang, 1989; Barriere and Turcotte, 1994;Sornette, 1992; Huang et al, 1996; Carlson et al, 1991; Olami et al, 1992; Blanter and Shnirman, 1996; Blanter et al, 1997;Blanter and Shnirman, 1997]. A strong advantage of this approach consists in the possibility to determine the relation between SOC and other forms of system behavior and to evaluate conditions of the transition from other behaviors to SOC.

In our previous work [Blanter and Shnirman, 1997] we have considered a simple hierarchical system of destruction representing different kinds of self-organised criticality. The self-organised criticality was governed by nonmonotone dependence of the failure occurring at (l+1)-th level on the number of distracted elements at previous level l. This nonmonotonicity give rise to a very complicated behavior characterised by self-organised criticality. In the present work we consider a similar kind of hierarchical systems and obtain SOC using heterogeneous conditions of the failure.

2. General description of the model.

Let us consider a hierarchical system of elements with branch number equal to 3 (Fig. 1). Each element of a higher level l+1 corresponds to a group of three elements of the previous level l. Elements of the system have two possible states, broken or unbroken. Element in a broken state is called as a defect. The state of an element of level l+1 is determined by the number of defects in the relevant group of three element of the previous level l. Thus, the density of defects at level l+1 can be expressed as follows:

$$p(l+1) = F(p(l))$$

Here the function F will be referred to as a transition function. Thus, the behaviour of the system depends on the transition function F and the initial density of defects at the first level of the system p(1).

3. Model behavior.

Below we consider various examples of transition functions F which correspond to different kinds of the behavior of the system.

3.1. Case of stability.

Let us consider a system where a group of three elements of level l, corresponding to a defect of the higher level l+1, contains exactly three defects. The transition function in this case will be:

$$F(p) = p^3$$

The function F is plotted in Fig.2a. It has two fixed points: p=0 and p=1. The former point p=0 is stable, the latter p=1 unstable. For each value of initial density p<1, densities of defects p(l) tend to zero, as level l increases (Fig.2b). It means that any perturbation appeared at the first level is damped for higher levels. The state of highest levels remains unchanged. This kind of behavior is referred to as *stability*.

3.2 Case of catastrophe.

Let us consider a system where a group of three elements of level l, corresponding to a defect of the higher level l+1, contains one or more defects. The relevant transition function can be expressed as follows:

$$F(p) = 1 - (1-p)^3$$

The function is plotted on Fig.3a. It has two fixed points: p=0 and p=1. The former point p=0 is unstable, the latter p=1 is stable. For each value of initial density p>0, densities of defects p(l) tend to 1, as level l increases (Fig.3b). Thus, for each positive perturbation of the first level all elements at level l will be broken if l is large enough. This kind of behavior is referred to as *catastrophe*.

3.3. Case of unstable criticality.

Let us consider a system where a group of three elements of level l, corresponding to a defect of the higher level l+1, contains two or more defects. The relevant transition function will be:

$$F(p) = 3p^2(1-p) + p^3$$

This function is plotted in Fig.4a. It has three fixed points: p=0, p=1/2 and p=1. Two of these (p=0 and p=1) are stable, the while p=1/2 is unstable. For initial density p(1)<1/2 the densities of defects p(l) tend to zero when level l grows; for p(1)>1/2 the

densities p(l) tend to unity, as l increases. The point p(1)=1/2 is critical. For each level l the density of defects p(l)=1/2, if p(1)=1/2 (Fig.4b).

Let us define a magnitude-frequency relation for this system. The number of defects at level l may be expressed as follows:

$$N(l) = 3^{L-l}\, p(l)$$

The magnitude of defect linearly depends on level number:

$$M(l) = l \lg 3$$

Thus, the magnitude-frequency relation has the following form:

$$\lg N(l) = -M(l) + \lg p(l) + const$$

At the critical point p(1)=1/2 the magnitude-frequency relation is linear. For the region p(1)<1/2 it has a downward bend (Fig.4c). At the unstable critical point p=1/2 there is a phase transition from stability to catastrophe. This case is referred to as the *unstable criticality.*

3.4. Mixed case of stable criticality (SOC).

Let us consider a composition of two cases described above. There are two kinds of elements in the system. Some elements are in the defect state if there are exactly three defects in the relevant group of the previous level. Others are in the defect state if there are one or more defects in the relevant group. If the number of elements of the first kind is equal to the number of elements of the second kind for each level, then the transition function will be the following:

$$F(p) = \frac{1}{2}(1 - (1 - p)^3) + \frac{1}{2}p^3$$

The function F is plotted in Fig.5a. It has three fixed points: p=0, p=1/2 and p=1. The point p=1/2 is stable, the other two are unstable. For each value of the initial density of defects p(1) densities p(l) tend to 1/2 as level l increases (Fig.5b). Thus there exist a nontrivial constant failure for all levels l of the system if l is large enough. The corresponding magnitude-frequency relation has a linear form that is similar to critical behavior. But in contrast to previous case critical behavior is obtained for all values of initial density p(1). So this case may be referred to as the *stable criticality.*

4. General mixed system.

Let us consider a model which is a generalisation of all systems described above. A hierarchical system is supposed to contain three kinds of elements. Elements of i-th type (i=1,2,3) become defects if there are i or more defects in the relevant group of three elements of the previous level. Let us denote the concentration of elements of i-th type as a_i: $a_1 + a_2 + a_3 = 1$.The transition function may expressed as follows:

$$F(p) = a_1(1-(1-p)^3) + a_2(3p^2(1-p) + p^3) + a_3p^3$$

It is obvious, that all these types of system behavior are particular cases of this general form. Only two from three concentrations ai are independent. The diagram of the behavior of the system for different values of concentrations a1 and a2 is plotted on Fig.6. Four parametric regions of system behavior are obtained: stability; catastrophe; unstable and stable criticality (SOC).

5. Conclusions and discussion.

We have showed that the simplest hierarchical system of static failure exhibits self-organised criticality as a result of heterogeneity in the scaling transition conditions of the failure. Parameters a_i governing the mixture of different kinds of elements determine the degree of heterogeneity of this model. To obtain the stable criticality the heterogeneity has to be strong enough (Fig. 6).

Both stable and unstable criticality are realised in the behaviour of our model. A transition from one case to another may be effect by changing the mixing parameters a_i. Let us suppose that a similar transition dynamically appears in real seismicity. Then the properties of seismicity preceding a catastrophic earthquake will vary in time according to the type of criticality observed. In a case of unstable criticality the development of the catastrophe is preceding by an upward bend of the magnitude-frequency relation [Narkunskaya and Shnirman, 1994]. In a case of stable criticality the increasing probability of a strong event is connected with the total increase of seismic activity similar for all magnitude ranges. A successful algorithm of earthquake prediction is to take into account this kind of variations of seismic properties .

Acknowledgements. The present work was supported by INTAS Foundation (project code INTAS-93-457) and by NSF (project code EAR 94-23818).

References:

Bak, P. and C. Tang. (1989). *Earthquakes as a self-organized critical phenomenon.* J. Geophys. Res., **94**, 15635-15637.

Bak, P.,C. Tang, and K. Weisenfeld (1988) *Self-organized criticality.* // hys. Rev. A. **38**, 364-374.

Barriere, B. and D. L. Turcotte.*Seismicity and self-organized criticality.* Phys. Rev. **49**, 1151-1160.

Blanter, E. M. and M. G. Shnirman, (1996).*Self-organized criticality in hierarchical model of defects development.* Phys. Rev. E. **53**, 3408

Blanter, E. M., M. G. Shnirman, J. -L. Le Mouël and C. J. Allégre, (1997). *Scaling Laws in Blocks Dynamics and Dynamic Self-organized Criticality.* Phys. Earth. Planet. Int. **99**, 295.

Blanter, E. M. and M. G. Shnirman, (1997). *Simple Hierarchical Systems: Stability, SOC and Catastrophic Behavior.* Phys. Rev. E. **55**, 6397-6403.

Carlson, J. M., J. S. Langer, B. E. Shaw and C. Tang. (1991) *Intrinsic properties of a Burridge-Knopoff model of an earthquake fault.* Phys. Rev. A, **44**, 884-897.

Ito, K. (1992). *Towards a new view of earthquakes phenomena.* PAGEOPH, **138**, 531-548.

Huang Y., H. Saleur, C. G. Sammis and D. Sornette, *Precursors, aftershocks, criticality and self-organized criticality.* preprint 9601065.

Narkunskaya, G. S. and M. G. Shnirman, (1994), *On an Algorithm of Earthquake Prediction,* in: Computational Seismology and Geodynamics,Vol.**1**: 20-25 (American Geophysical Union, Washington, D.C.)

Olami, Z. H. Feder and K. Christensen, (1992) *Self-organized criticality in a non-conservative cellular automaton modeling earthquakes.* Phys. Rev. Lett., **68**, 1244-1247.

Sornette, A., Ph. Davy, and D. Sornette. (1990) *Structuration of Lithosphere in Plate Tectonics as a self-organized Critical Phenomenon.* J.Geophys.Res., **95**, 17353-17361.

Sornette, A. and D. Sornette. (1989) *Self-organized Criticality and Earthquakes.* Europhys.Lett., **9**, 197-202.

Sornette, D. (1992) *Critical Phase-Transition Made Self-Organized - A Dynamic System Feedback Mechanism for Self-Organized Criticality.* Journal de Physique I, **2**, N 11, 2065-2073.

Figure captions

FIGURE 1. Hierarchical system of elements with branch number equal to 3.

FIGURE 2. Case of stability:
(a) transition function (solid line);
(b) densities of defects p(1)=0.99.

FIGURE 3. Case of catastrophe:
(a) transition function (solid line);
(b) densities of defects p(1)=0.01.

FIGURE 4. Unstable criticality:
(a) transition function (solid line);
(b) densities of defects:
p(1)=0.1 - (1); p(1)=0.5 - (2); p(1)=0.7 - (3);
(c) magnitude-frequency relation:
p(1)=0.1 - (1); p(1)=0.5 - (2).

FIGURE 5. Stable criticality (SOC):
(a) transition function (solid line);
(b) densities of defects:
p(1)=0.3 - (1); p(1)=0.5 - (2); p(1)=0.7 - (3);

FIGURE 6. Parametric areas of different kinds of system behavior.

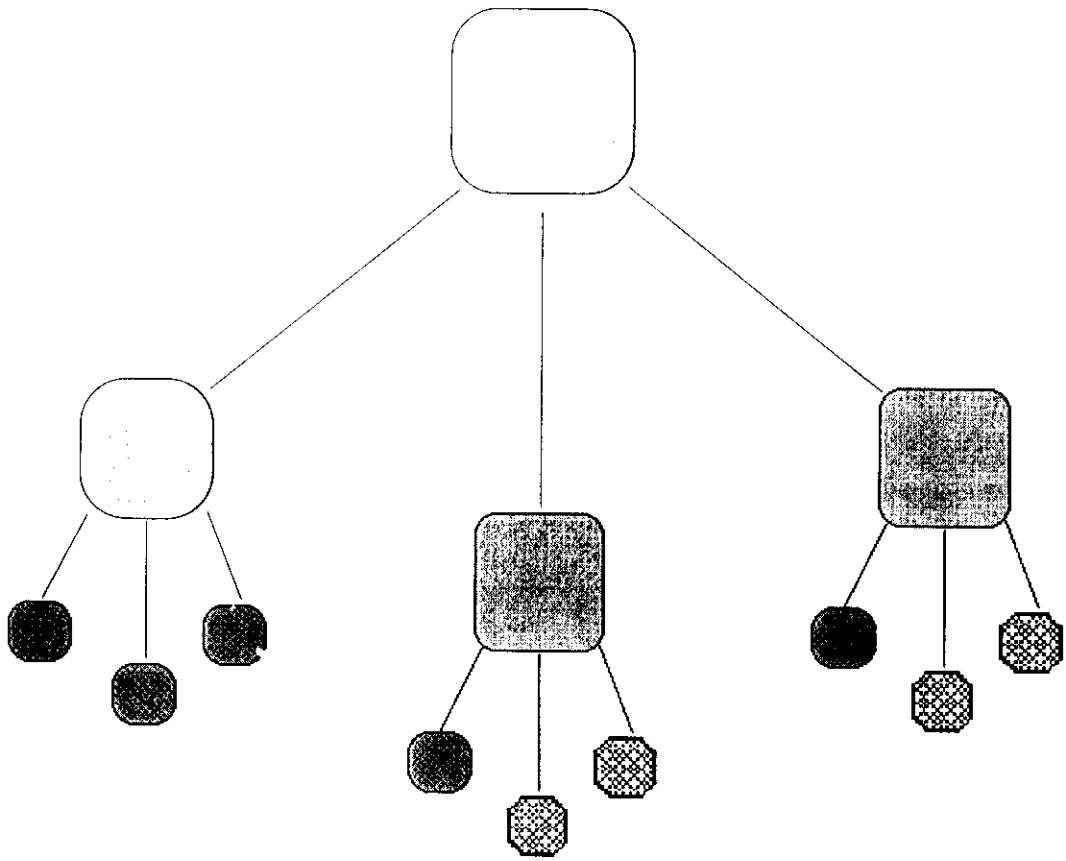

Fig. 1. Hierarchical system of elements with branch number equal to 3.

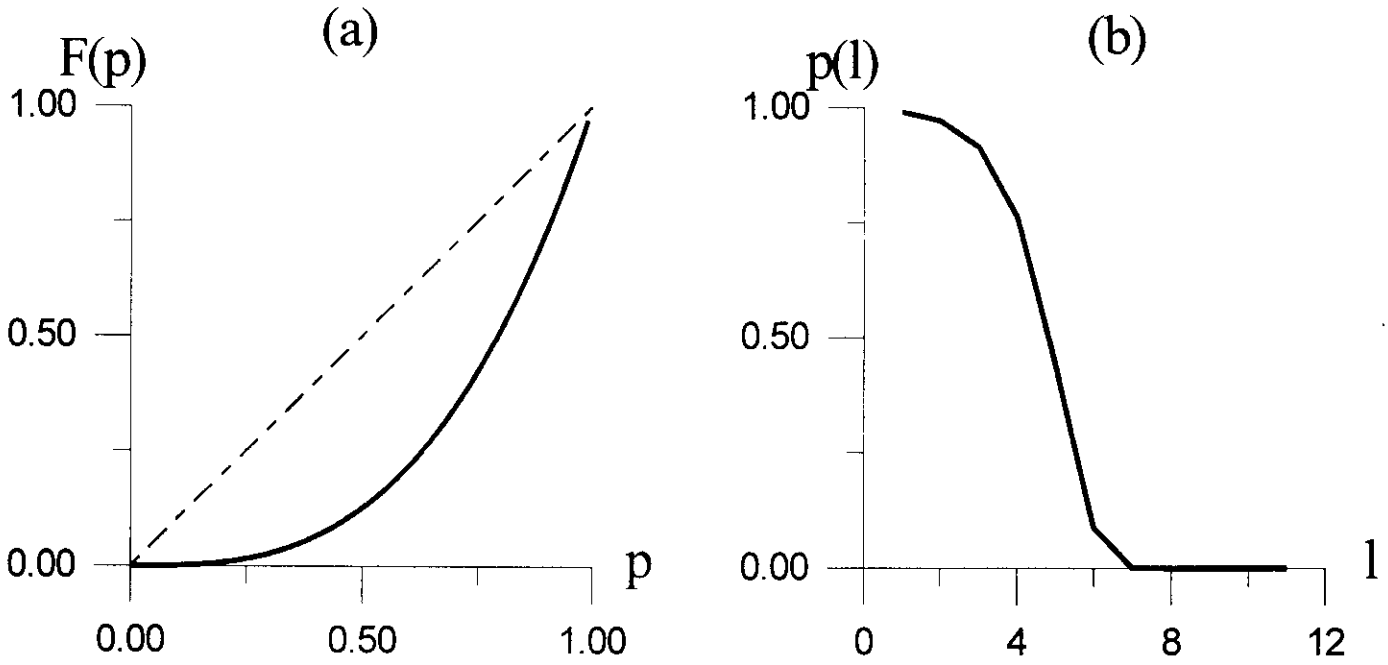

Fig.2 Case of stability:
(a) --- transition function (solid line);
(b) --- densities of defects p(1)=0.99.

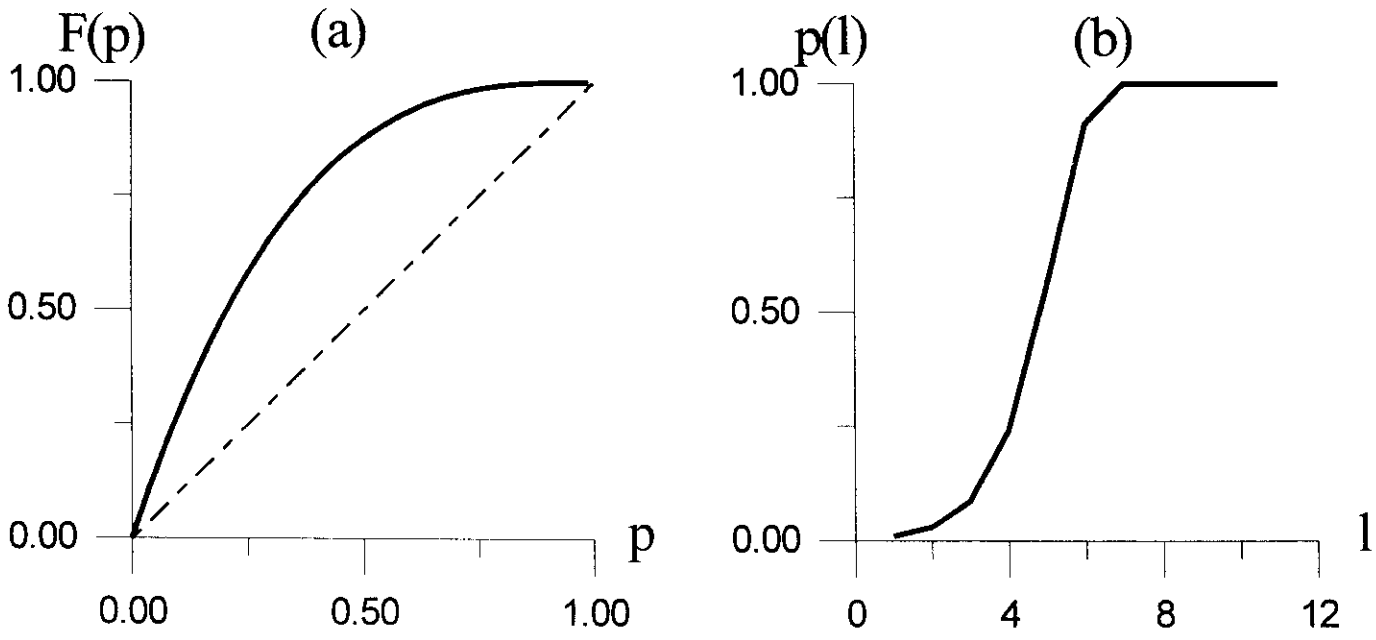

Fig.3 Case of catastrophe:
(a) --- transition function (solid line);
(b) --- densities of defects p(1)=0.01.

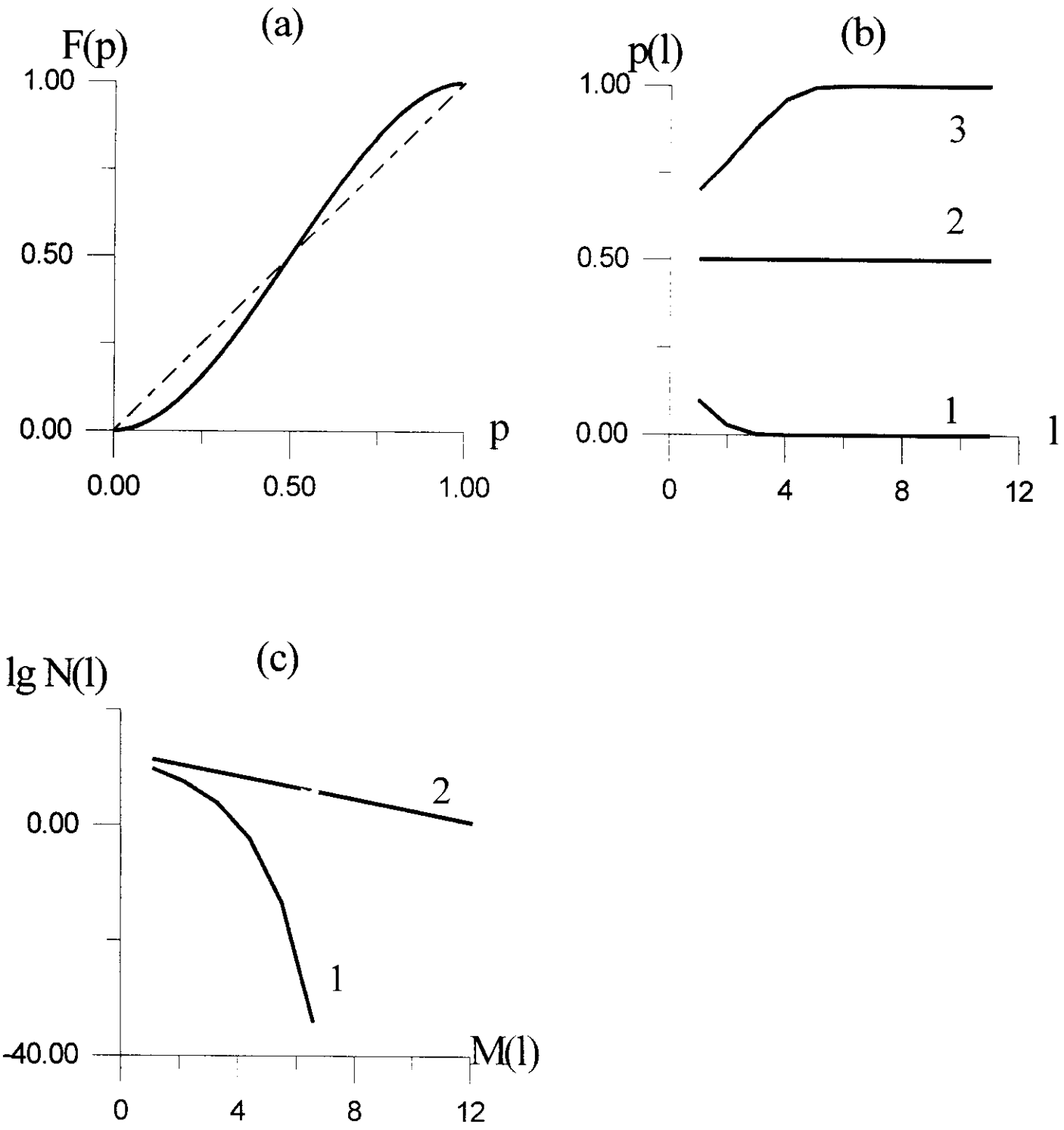

Fig.4 Unstable criticality:
(a) --- transition function (solid line);
(b) --- densities of defects:
p(1)=0.1 --- (1); p(1)=0.5 --- (2); p(1)=0.7 --- (3).
(c) --- magnitude-frequency relation:
p(1)=0.1 --- (1); p(1)=0.5 --- (2).

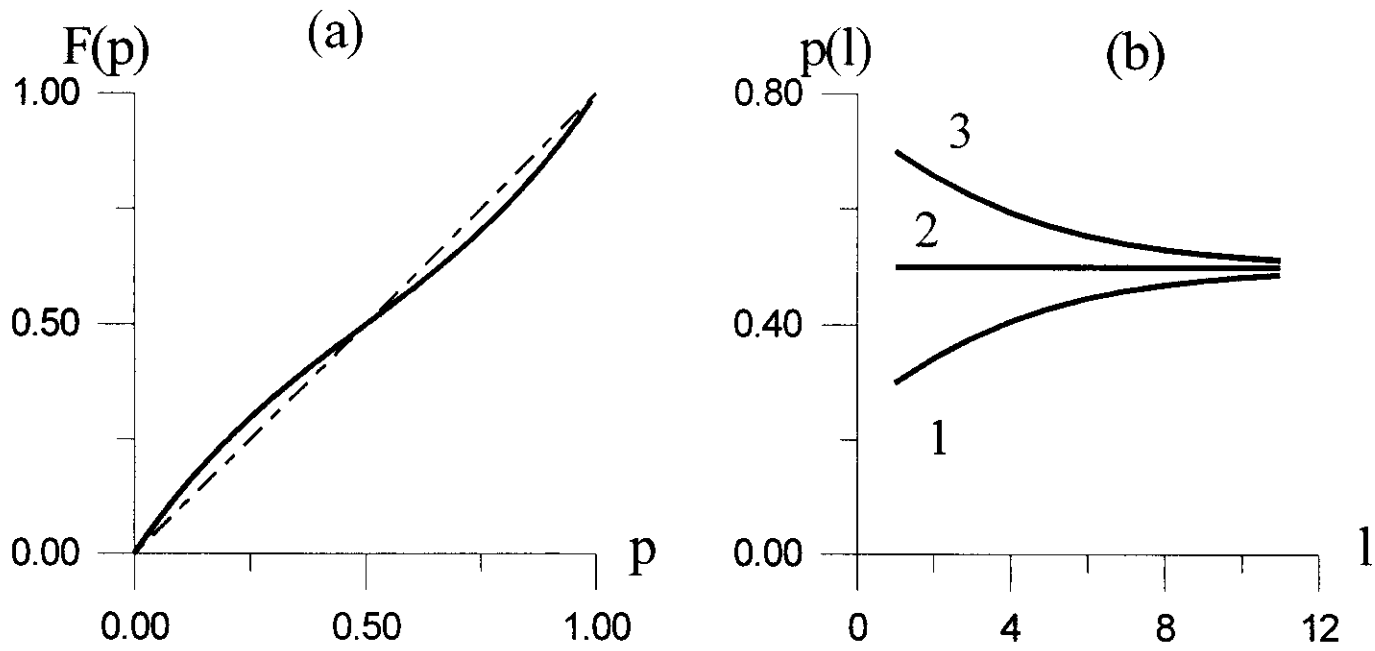

Fig.5 Stable criticality (SOC):
(a) --- transition function (solid line);
(b) --- densities of defects
p(1)=0.3 --- (1); p(1)=0.5 --- (2); p(1)=0.7:.

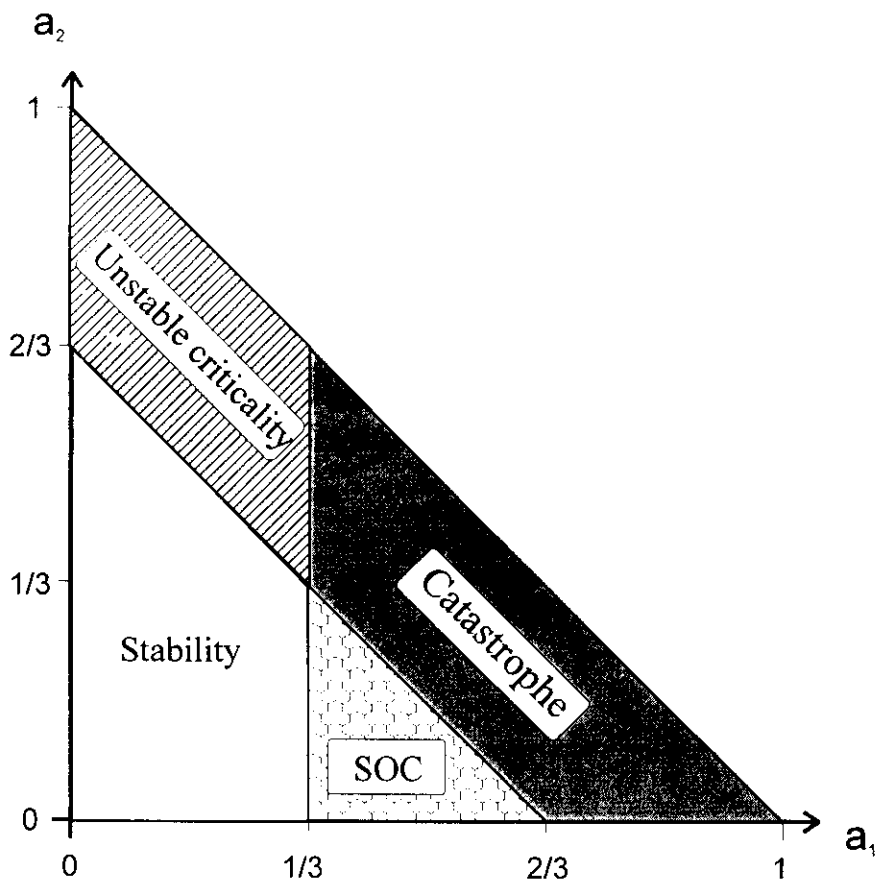

Fig 6. Parametric areas of different kinds of system behavior

New technique for the reconstruction of stress release and deformation fields in the earthquake prone area

A.V.Lander, B.G.Bukchin, A.V.Kiryushin

Expansion of data base: The larger set of data on stress release and deformation fields generated by the earthquakes consists of polarities of P-waves first arrivals. Over 3 million polarity readings for about 350 thousand earthquakes are by now accumulated worldwide. The traditional method requires that fault plane solutions are determined first. That is possible only for 10% of the earthquakes with a sufficient number (20 or more) of polarity reports (Figure 1). We will use an alternative methodology (*Lander et al.,1996*) based on the description of stress and strain tensors as probability distributions in a five-dimensional linear space. This methodology allows to use the earthquakes for which reliable determination of a fault plane solution is impossible (even those with a single polarity reported). Thus at least 5 times more data can be used.

Main features of the technique. In formal terms the method relies on a description of earthquake mechanisms (the **m** tensor) and seismogenic strain (the **M** tensor) as vectors in a five-dimensional linear space of three-dimensional symmetrical matrices with zero trace. The direction of a 5D vector describes the principal elements of source geometry, the absolute value of the vector being source intensity. Earthquake mechanisms are found from $l(\mathbf{m})$, the likelihood function of the 5d-vector (moment tensor); after normalization this can be treated as a posterior probability distribution of the solution

$$P_k(\mathbf{m}) = l(\mathbf{m}) \Big/ \int l(\mathbf{m}) d\mathbf{m}$$

Here and below any integral (replaced by a sum in calculations) is approximately computed on a five-dimensional unit sphere, k - is the number of earthquake.

$$\langle \mathbf{m} \rangle_k = \int \mathbf{m} P_k(\mathbf{m}) d\mathbf{m}$$

$$\langle \mathbf{B} \rangle_k = \int \mathbf{m}\,\mathbf{m}^{\mathrm{T}} P_k(\mathbf{m}) d\mathbf{m} - \langle \mathbf{m} \rangle_k \langle \mathbf{m} \rangle_k^{\mathrm{T}}$$

The distribution $P_k(\mathbf{m})$ can be formally calculated even for an earthquake with a single first motion observation. In that case the mean tensor will be only slightly different from zero, but when such mean vectors for earthquakes occurring in a region are summed, some general patterns in its tectonic (deformational) evolution may gradually emerge.

The strain tensor **m** described by the probability distribution $P_k(\mathbf{m})$ is ascribed to a volume surrounding the k-th hypocenter $\mathbf{r}_k$ with characteristic radius R_k. The strain amplitude smoothly falls off from the center to the edges of the volume according to a fixed law $D((\mathbf{r}-\mathbf{r}_k)/R_k)$.

Assuming the $\mathbf{m}_k$ for different earthquakes to be independent, one finds the total strain at an arbitrary point **r** as

$$\mathbf{M}(\mathbf{r}) = \sum_k D((\mathbf{r} - \mathbf{r}_k)/R_k) \langle \mathbf{m} \rangle_k$$

and the "error matrix" as

$$\mathbf{B}(\mathbf{r}) = \sum_k D((\mathbf{r} - \mathbf{r}_k) / R_k)\mathbf{B}_k$$

The strain amplitude at **r** is defined to be the absolute value of the five-dimensional vector $|\mathbf{M}(\mathbf{r})|$.

The uncertainty is estimated, in particular, by using the typical signal/noise ratio

$$q(\mathbf{r}) = \left\{ |\mathbf{M}(\mathbf{r})| / \left[\mathrm{Trace}\{\mathbf{B}(\mathbf{r})\} / 5 \right] \right\}^{1/2}$$

Horizontal strain on the horizontal plane is given by the tensor **h**(2x2), which is a minor of the total strain tensor **M** (in matrix form) in the relevant basis.

The tensor **h** has a nonzero trace in the general case, where areas of compression (Trace **h** < 0) and extension (Trace **h** > 0) exist in the horizontal plane. From the requirement Trace **M** = 0 it follows that the value of Trace **h** taken with the opposite sign is equal to the vertical strain component M_{zz} of the horizontal plane. For this reason areas of general horizontal compression in this model are also zones of subsidence, and areas of extension are zones of uplift.

Reliability of the methodology. We set up a compact (≈ 100 Mb) data base to be used for plotting maps of seismogenic strain; the data base includes:

- ISC, NEIC catalogs and bulletins for 1964-1996;
- CMT catalog (Harvard, USGS) for 1976 until present time;
- Catalogs of fault plane solutions for 1964-1996 (the solutions have been formally revised for 334,786 events such that at least one first motion observation is available in the catalogs).

A library of subroutines has been made to provide simple and rapid access to any data set; the library consists of original software. Software has been developed implementing the statistical technique (outlined above) for reconstructing seismogenic strain fields; it uses first motion signs, but does not require reliable mechanisms of individual earthquakes.

The above data and technique have been used to obtain digital maps showing the distribution of the seismogenic strain tensor **M** over the Earth's surface (the typical radius of map smoothing is 400 km). Similar maps for various scalar characteristics of the tensor field were calculated, for instance: strain amplitude |**M**|, Mzz component which characterizes the amplitude of horizontal compression (extension), the quantity $\{(Mxx-Myy)^2+2M^2xy\}$, which characterizes the amplitude of the deviatoric component of the tensor (intensity of shearing movements) etc.

Maps have been made both for various types of raw data (CMT, Fault Plane Solutions) and for various seismicity ranges (fixed magnitude ranges).

Three cumulative maps of the Mzz component of the strain tensor generated by earthquakes in Western Pacific, 1964-1997 are presented in Fig.2. The values of Mzz are normalized by the maximal value for each map. The maps are based on three different data types. Left and central maps are based on reliable data on seismic moment tensor (Harvard CMT) and fault plane solutions (M>5), respectively. *The map on the right is based on the data that are unsuitable for usual interpretation (events with less than 10 first motion*

polarities). However the distribution of relative deformations for major tectonic features is in overall agreement on all three maps. This shows that a great amount of useful information on tectonic processes is hidden in polarity data which were never touched.

The results implies that following problems can be studied using the tecnique: (i) To find quantitative statistical relations between the fields generated by earthquakes in different magnitude ranges (pilot studies show intriguing stable differences in these fields). (ii) To study the evolution of strain field prior to large earthquakes. (iii) To find an operator transforming the tensor field of deformations considered to the vector field of modern tectonic movements. For determination of this operator we will use the data on major plate boundaries where tectonic movements are relatively clear.

References

Lander, A. V., B. G. Bukchin, D. V. Droznin, and A. V. Kiryushin, The tectonic enviroment and source parameters of the Khailino, Koryakiya earthquake of March 8, 1991: Does a Beringia plate exist? in *Computational Seismology and Geodynamics, Vol. 3*, D.K.Chowdhury, ed., pp. 80-96, Am. Geophys. Un., Washington, D.C., 1996.

Distribution of earthquakes
vs.
number of the first arrival polarity reports

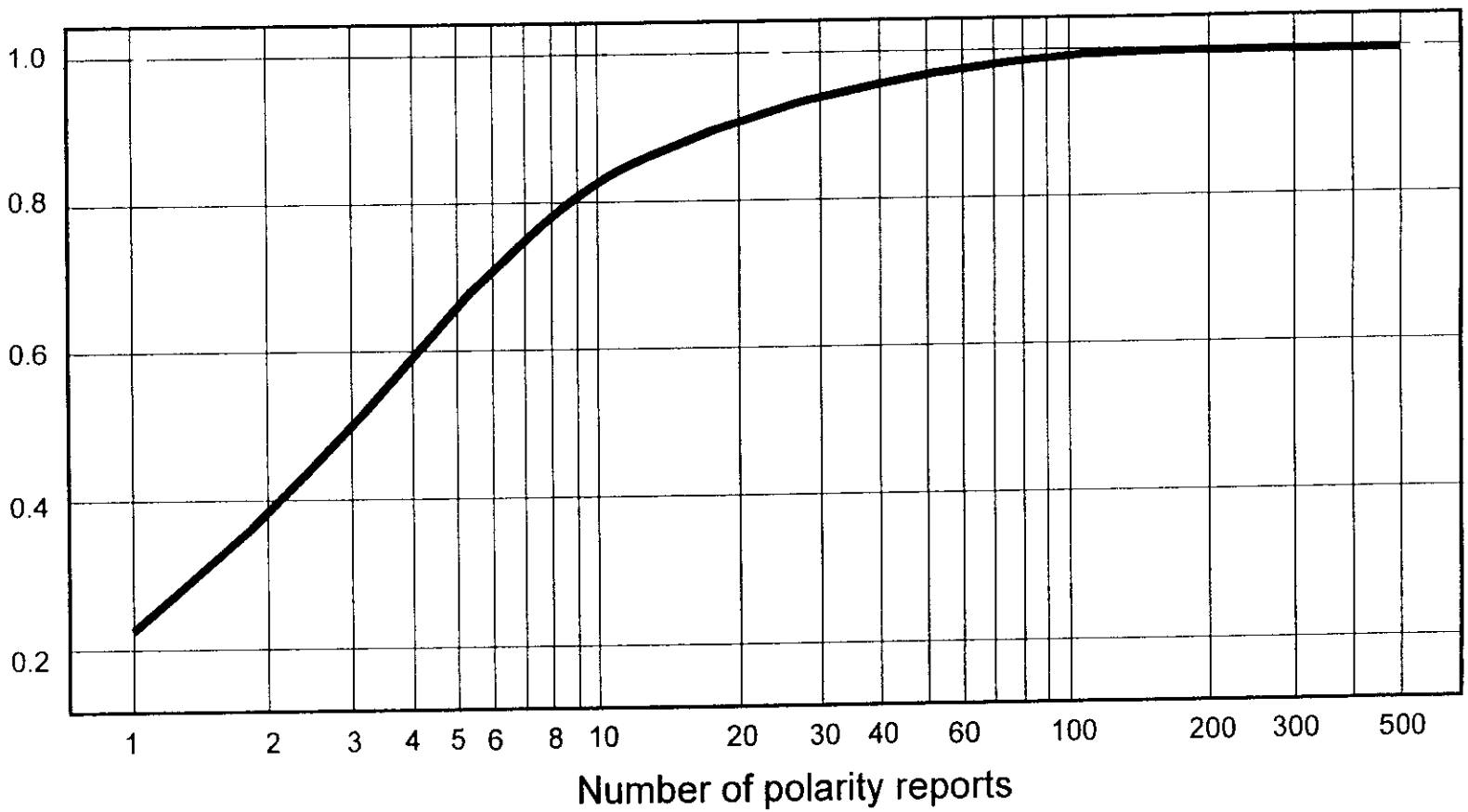

Fig. 1. Lander, Bukchin, and Kiryushin, 1997 (*lander@mitp.rssi.ru*)

Normalized intensity of vertical motion, realized by earthquakes (ZZ component of cumulative deformation tensor)

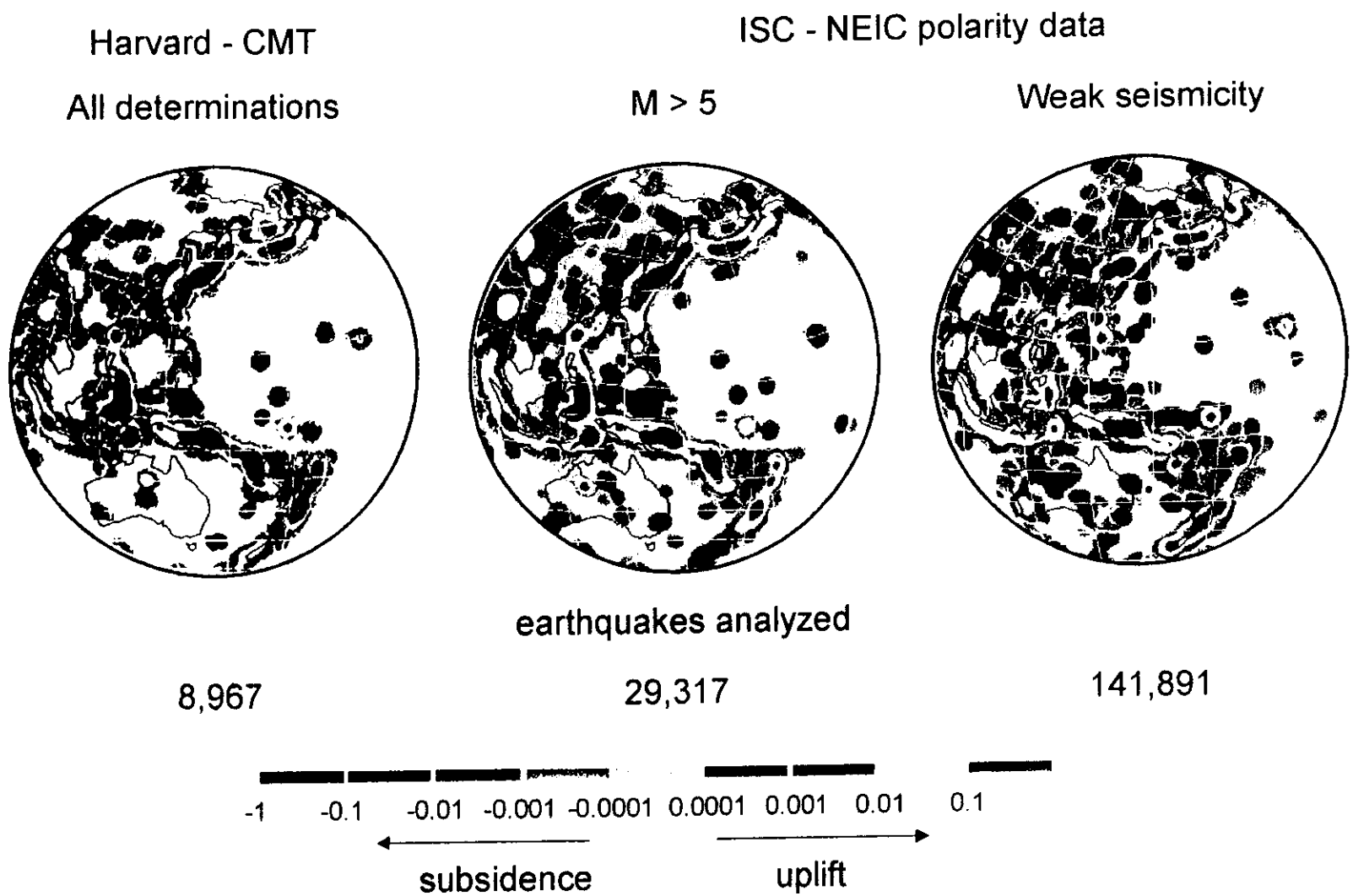

Fig.2. Bukchin, Lander, and Kiryushin, 1997 (*lander@mitp.rssi.ru*)

I.Primakov

Type of trajectory instability in coordinate phase space for movable disk model of lithosphere.

When one analyses the behavior of solutions of complex dynamic system it is natural to ask what is the type of there instability if any. *The movable disk model of lithosphere* is an example of such system. Often the question of instability is discussed in terms of Lyapunov's exponents. Let us remind that Lyapunov's exponent $\lambda_{x(t)}$ of the solution $x(t)$ of linear system $\dot{x} = A(t)x$ is defined as:

$$\lambda_{x(t)} = \overline{\lim_{t \to +\infty}} \frac{1}{t} \ln|x(t)|$$

Even the existence of finite $\lambda_{x(t)}$ for nonlinear system is not obligatory.
In our particular case trajectories in the coordinate phase space are finite, so formally defined Lyapunov's exponents are nonpositive for all the trajectories.
That by no means exclude the question about the type of increase of $\ln|x(t)|$ when $0 << t << \infty$.
Our goal was not to study directly the *asymptotic* stability of solutions of our nonlinear system. We were rather interested in numeric study of the velocity of deviation of projections of trajectories on coordinate space in intermediate time scale.
That was done in the following way. At first a stable configuration $\tilde{\boldsymbol{n}}_i$ of 60 disks was found and the evolution of coordinate trajectory $\boldsymbol{x}_0$ of the length about 10^6 was calculated. Then a set of similar trajectories $\boldsymbol{x}_i$ was obtained under the same external conditions from initial configurations $\tilde{\boldsymbol{n}}_i$ very close to $\tilde{\boldsymbol{n}}_i$.
Here we will not describe different methods of obtaining the deviated configurations $\tilde{\boldsymbol{n}}_i$.

So major interest is in the rate of increase of $\ln \Delta = \ln|x_i(t) - x_j(t)|$ when t is large enough but not tends to infinity.

Basic results:

- $\ln \Delta \approx 1.5 \div 2 \ln t$, i.e. increase of is rather as square then exponential. The fact is well illustrated by Fig. 1.
- There is no monotonous dependence between $|c_i - c_j|$ and Δ when t is big enough.

Figure captions

Fig. 1. Power law instability in a movable disks model of seismicity.

Δ is the distance from a perturbed to the initial trajectory.

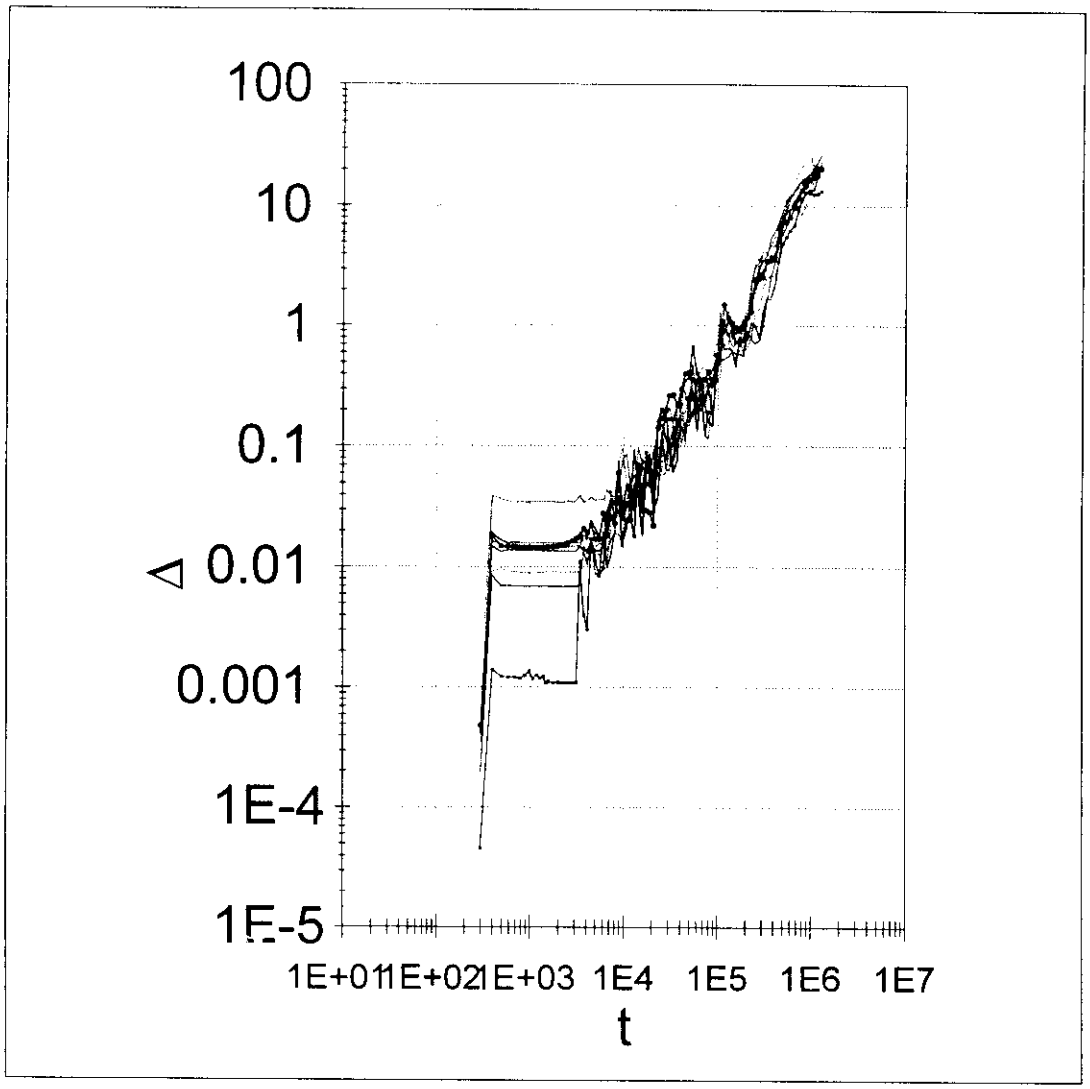

Fig. 1. Power law instability in a movable disks model of seismicity.

Δ is the distance from a perturbed to the initial trajectory.

PROGRESS REPORT

V.F.Pisarenko, A.A.Lyubushin

PREDICTABILITY IN CELLULAR AUTOMATA: FOREST-FIRE AND OTHER LATTICE MODELS

ABSTRACT

The forest-fire models are studied in particular in context of seismicity. In addition to known properties of self-organized criticality of forest-fire models several new features of these cellular automata were found. A spectral peak in energy dissipation process was discovered in intermediate frequency range. This periodic component exhibits coherent behavior in different space sub-parts of the model. The Hurst exponent H determining self-affine fractal dimension of energy process was measured in a moving time window. The fractal dimension was about 1.1. Some oscillations of energy process prior to large fires were observed both with increasing frequency and with decreasing one. These oscillations were found with the help of wavelet analysis. Whether the oscillations with increasing frequency correspond to log-periodic form suggested by the Discrete Scale Invariance theory is to be studied in further investigations. A new approach to prediction of cellular automata is suggested: prediction of sites where large events are impossible (prediction of "non-fires"). Several statistics of such prediction for forest-fire model are derived. Some problems for future investigation of forest-fire models are enumerated.

Key words: *cellular automation, forest-fire model, log-periodic oscillations, wavelet analysis, canonical coherences, collective behavior.*

INTRODUCTION

Discrete models called cellular automata (CA) have received a lot of attention recently. They are being used intensively for studying non-linear interactive dynamical systems such as turbulence, rock fracturing, seismicity and many others. Of course, these models are not believed to be a realistic representation of any particular system: they capture only some general properties of typical behavior and may provide a guideline for further systematic study of natural systems.

The most famous CA of such type is the sand-pile model suggested by Wiesenfeld, Tang and Bak [1]. As a result of studying this model a very important and informative notion of self-organized criticality (SOC) was discovered. Later on, this model was modified so that it can be interpreted as a discrete cellular version of the well known spring-block model of seismicity by Burridge and Knopoff [2]-[3]. The spring-block models have been recognized as an informative and useful tool for investigation of seismicity (see e.g. the review [4] and references cited therein).

Recently D.Turcotte stressed the importance of studying the class of so-called forest-fire (FF) models in particular in context of seismicity [5]. These models generally exhibit SOC and are considered useful not only in ecology but in turbulence [6], spread of diseases and other applications. Unfortunately, their seismic applications are scarce if any.

and are considered useful not only in ecology but in turbulence [6], spread of diseases and other applications. Unfortunately, their seismic applications are scarce if any.

We investigate in this paper the FF models first of all with a view to find some new features of the SOC systems that could help to analyze their evolution and predictability. Several peculiarities of the FF model were observed.

A spectral peak was found in the FF process. The existence of such peak is quite unusual for SOC processes whose spectrum has as a rule the *1/f* form [1]. The periodic component has non-zero coefficients of coherence for different space sub-domains of the model. The physical meaning of this spectral peak needs further investigations.

We sought for log-periodic oscillations prior to large fires similar to those that had been found in some lattice models and natural processes [7]-[9]. In contrast to the cited papers where some particular parametric form of oscillations was assumed we used the general non-parametric wavelet analysis. A distinct oscillations with changing periods (both accelerating and decelerating) were observed in some realizations of the FF process. This interesting phenomenon needs further investigations.

A new approach to prediction of future states of the system was suggested, namely, prediction of places where no fire is possible in the next time step (prediction of "non-earthquakes"). Some statistics of such prediction were derived. Perhaps, this kind of prediction will be of some use in seismic risk assessment. The search of precursors of non-earthquakes in CA models should be continued in the same manner as it is done for precursors of earthquakes.

Summarizing our preliminary experience with FF models we conclude that they can be considered as a promising model for the study of seismicity. Present paper should be viewed rather as a program for future investigations than a report of a completed research.

FOREST-FIRE MODELS

We consider a class of models that are referred to as forest-fire models [5]-[6]. In a rectangular grid of sites each site can be occupied either by a tree or be empty. At each time-step either a tree is randomly planted on a site or a match is dropped on the site. The sparkling period T indicates how many trees are planted before a match is dropped. If sparkling period T is equal, say, to 100 then 99 trees are planted (or are attempted to be planted) before a match is dropped.

Histogram for sparkling period T=25 is shown on Fig.1. Some range of linear behavior of histograms in double-log scale can be selected. The histogram on Fig.1 clearly illustrate so-called "Yellowstone Park" effect. After a massive forest fire covered a significant fraction of the Yellowstone National Park, it was argued that if smaller fires had been allowed to burn, the massive forest fire could have been prevented. Allowing small fires to burn is equivalent to having a smaller sparkling period. The results given in Fig.1 illustrate how the small fires prevent the occurrence of catastrophic fires that burn essentially the entire model forest. "Yellowstone Park" effect can be considered as an analog to water pumping into deep wells discharging rock stress by small shocks.

Let us call the number of burned trees in a fire by "energy" and consider cumulative energy $E(t)$ dissipated by fires till the time t, computed with regular time step, which equals 100 time cycles. One time cycle means (T-1) randomly planted trees and one randomly thrown match. Spectra of $E(t)$ after removing a general linear trend are shown on Fig.2 for two different FF models: rectangular, 1024x32 (such a prolongated form was chosen in order to models effect similar to those on some long seismic fault), Fig.2a and square, 100x100,

Fig.2b. Almost linear behavior of the log-log spectra in low-frequency range is seen for both models. Such behavior is typical for SOC systems. But in addition to this usual feature one can observe distinct spectral peaks in the range of intermediate periods. These peaks differ for the two models. The value of this characteristic period can be tentatively interpreted as an averaged number of cycles, needed for covering the area of the model (1024x32) or (100x100) by randomly thrown matches. The peak amplitudes are noticeably less than low-frequency part of the process but, nevertheless, the existence of the peaks is out of any doubt. For comparison we have shown on Fig.2c the spectrum of cumulative energy for CA of Burridge-Knopoff type [10]. Nothing but linear behavior is seen on this figure.

Fig.3 illustrates results of estimating a time-frequency evolution of some measure of collective behavior between 4 parts of the lattice 1024x32, sense of which is described below.

Lets consider a 4-dimensional time series:

$$\vec{Z}(t)=(Z_1(t),Z_2(t),Z_3(t),Z_4(t))^T \qquad (1)$$

each component $Z_k(t)$ of which represents a cumulative value of energy, outcoming from 4 non-overlapping parts of the lattice, with "x-coordinates", laying in diapasons 1-255, 256-511, 512-767, 768-1024. Each event is considered to have a spatial coordinate, which equals to centers of mass of the cluster of nodes (trees), involved into the event. So, having an artificial catalog, in which we store energy of event, its time moment and centers of mass of its cluster, we can estimate an energy output from any part of the lattice during any time interval. This energy output is calculated in cumulative form with some regular time step Δt, which usually equals 100 time cycles. That is why a time value t in (1) is discrete. After a time interval, for which we calculate the energy output from the considered part of the lattice, is finished, a general linear trend from the curve of cumulative energy is removed and the residuals (deflections from the linear trend) constitutes a time series for further analysis. By this method we can create a number of multi-dimensional time series $\vec{Z}(t)$, representing peculiarities of energy output from a number of parts of the "big" lattice.

Now we want to describe effects of interactions between some two different parts of the vector $\vec{Z}(t)$. Let the l-dimensional vector $\vec{Z}(t)$ (for the case (1) l=4) could be splitted into two vectors: m-dimensional vector $\vec{X}(t)$ and n-dimensional vector $\vec{Y}(t)$, $l=n+m$ (without restriction of generality let $m \le n$).. Let now ask a question: how to describe the interaction between two lattice regions, represented by these two series, in various frequency bands.

To answer questions of such a kind, a notion of *maximal canonical coherence* is useful [11,12]. Lets consider the matrix, which is composed as a following product of inverted spectral and cross-spectral matrices:

$$U(\omega) = S_{xx}^{-1}(\omega) \cdot S_{xy}(\omega) \cdot S_{yy}^{-1}(\omega) \cdot S_{yx}(\omega) \qquad (2)$$

It is seen that when both series are not vectors but scalars, then formula (2) becomes a usual squared spectrum of coherence. It could be shown that eigenvalues of the matrix (2) are real, non-negative and ≤ 1. These eigenvalues have a sense of squared spectrum of coherence between some scalar time series, which are called *canonical components* of initial time series $\vec{X}(t)$ and $\vec{Y}(t)$. Let $\mu_1^2(\omega)$ be the maximal eigenvalue of the matrix (2) (i.e. the maximal canonical coherence). Then if for some values of frequency the maximal canonical coherence

increases considerably and approach the value of 1, it means that for this frequency the statistical relation between two vector time series is strong.

Let now introduce a notion of *by-component canonical coherence* $v_i^2(\omega)$ as a maximal canonical coherence in a situation, when time series $\vec{X}(t)$ is composed only from i-th scalar component of time series $\vec{Z}(t)$ (m=1) and $\vec{Y}(t)$ - from all *others* components of $\vec{Z}(t)$ (n=l-1). The value of $v_i^2(\omega)$ describes the "strength" of relation between variations with the frequency ω of i-th component and *a set of all others* components. Computing the average value of all by-component canonical coherences gives a spectral statistics which describes the "strength" of *joint relations* (a strength of collective behavior) between all components of $\vec{Z}(t)$ on a given frequency value ω :

$$\rho^2(\omega) = \frac{1}{l}\sum_{i=1}^{l} v_i^2(\omega) \tag{3}$$

It is evident that $0 \le \rho^2(\omega) \le 1$ and, hence, more close is the value of (3) to 1, more strong are effects of collective behavior of scalar components of $\vec{Z}(t)$ on a considered frequency ω .

Let τ be a time coordinate of moving time window, for example, its center or right-hand end (which is more convenient for prediction purposes), L be the number of samples in time window, Δt be the sampling time interval. Computing statistics $\rho^2(\omega)$ not over all interval of observation, but in a moving time window, we will obtain a two-parametrical function $\rho^2(\tau,\omega)$ Parameters of time window and the value of sampling time interval give a frequency band, which could be investigated with the help of statistics (3):

$$2\pi/((L-1)\Delta t) \le \omega \le \pi/\Delta t \tag{4}$$

Finally we are able to describe the Fig.3. It represents function $\rho(\tau,\omega)$ for 4-dimensional time series (1), calculated in moving time windows of the length 2048 "samples" (204800 time cycles), taking with mutual shift 512 "samples" (51200 time cycles). For estimating spectral matrices a vector autoregression model of the order=10 was used. A clear coherence stripe with amplitude about 0.4 is seen at the frequency corresponding to the peak on Fig.2a. Thus, we can conclude that energy dissipation process is coherent at this frequency in different space parts of the model. The physical meaning of this coherence needs further investigations.

LOG-PERIODIC OSCILLATIONS PRIOR TO LARGE FIRES

Log-periodic oscillations (LPO) of dissipated energy (or some other parameter) were observed for different CA and natural systems including seismicity, geochemical processes, acoustic emission and even stock market prices [7]-[9]. Their nature is still not quite clear. There exist some conjectures explaining their existence by self-similar cycles in the energy dissipation due to a negative feed-back.

The technique for extraction LPO from data, developed by Sornette et al. [7-9] consists in a parametric estimation with some prescribed signal form including logarithmically

accelerating frequency. This parametric form is derived from an assumption of a cyclic scaling (so-called discrete scale invariance (DSI)) in dissipation process. Such assumption has no clear physical basis so far, although one can believe the existence of negative feed-back in many natural processes. That is why we decided to try to detect a signal of arbitrary form preceding large event. We have used for this purpose the modern wavelet analysis that has proved its efficiency in similar problems [13]-[14].

Loosely speaking, wavelet technique gives a representation of a signal in form of a series of wavelets obtained by a scaling procedure. This representation is similar to the well-known time-frequency analysis but it is spatially and temporally adaptable, more parsimonious and efficient (see [13]-[14] for more details about wavelet technique). So-called the Daubechies wavelets of the 12-th order were used to analyze energy dissipation process, i.e. for time series of the type (1), calculated in a vicinity of several large fires with $E > 1000$ for the lattice area with x-coordinates ± 50 nodes around x-coordinate of center of masses of fire's cluster. Some results are shown on Fig.4. Different levels (1-11) correspond to different degrees of MRA (*Multi-Resolution Analysis*) or detailness. The Level 1 describes the most high-frequency parts of signal while the Level 11 characterizes one of the most smooth parts. The number of MRA-levels depends on the length of the series to be analyzed. If the series have N samples then the whole number of MRA-levels equals $(m-1)$, where m is the minimal integer number for which $N \le 2^m$

Horizontal axis on Fig.4 is time. Vertical axes show absolute value of coefficients in wavelet expansions for a given time. In order to diminish statistical fluctuations of wavelet coefficients' absolute values, they were averaged by smoothing time window with a radius = 256 "samples" (25600 time cycles). This operation is similar to the averaging of periodograms in usual spectral analysis. Because of finite time length of wavelet functions, which increase with MRA-level number m as 2^m, this operation is essential only for low values of m: on Fig.4 wavelet coefficient for $m>8$ could not be averaged by such a time window. This fact is also similar to usual spectral analysis, where long periodic components power could not be estimated by averaging periodograms. Because of the finite length of wavelet functions and using of time averaging, each value of wavelet coefficient on each MRA-level is obtained from some time interval, which could be named a *wavelet-packet length*. For convenient using for predictability purposes, time axis represents *right end* of wavelet-packets on each level.

Local maxima on Fig.4 correspond to large coefficients. The time of the largest event in analyzed interval is marked by dash line. We have connected maxima in adjacent Levels by a polygonal line. Since these maxima are not very pronounced this step is somewhat subjective. In further research more accurate statistical methods will be applied which should give more reliable results.

On Fig.4 one can discern two branches of time-moving maxima prior to the large event: descending and ascending. They can be interpreted as oscillations with decreasing frequency and with increasing frequency correspondingly. Whether the ascending branch has a linear growth of frequency with time or a log-periodic form as it follows from DSI assumption is difficult to judge now because of low signal-noise ratio. More accurate analysis will permit answer this question. The descending branch of oscillations was not observed earlier.

On Fig.4 one can see another curious detail: a descending oscillation branch AFTER the main event. It can be connected with post-fire effects (analog of aftershocks). Similar effects were observed for stock market prices [9]. It should be noticed that oscillations described above were observed not for all large events. This question should be clarified by further investigations.

Now we are going to describe two more properties of FF models observed in our numerical experiments. The first one consists in spatial alternation of large fires. On Fig.5 the spatio-temporal trajectory of large fires is shown. Vertical axis corresponds to the larger ("X") side (1024) of our rectangular model (1024x32) which is denoted as X-coordinate. We see that there is a noticeable alternation of X-coordinate in time. More subtle statistical analysis will permit to evaluate the usefulness of this alternation for predictive purposes.

The second property is connected with the Hurst exponent H [15], [16]. This exponent determines the rate of growth of normalized range $R(t)$ with time:

$$R(t) \approx t^{H}$$

where $R(t)$ is equal to ratio of difference between max and min of the process to empirical standard deviation measured on time interval $[0,t]$. The Hurst exponent has proved to be an informative parameter in many natural processes (see e.g. [16]). Especially it is useful for chaotic processes of the Brownian motion type. The exponent H is defined in the range $0 < H < 1$. The value $H = 1/2$ corresponds to the Brownian motion itself while other possible values correspond to so-called fractional Brownian motion (fractional derivatives of the Brownian motion, positive or negative) [16]. The range $1/2 < H < 1$ gives rise to processes with persistence while the range $0 < H < 1/2$ gives rise to antipersistence. We measured the Hurst exponent in a moving time window for energy dissipation process (i.e. for series of the type (1)) in FF-models.

The result is shown on Fig.6, which represents the evaluation of the Hurst exponents for the "most seismic" half of the lattice for X-coordinates diapason 512-1024, calculated in moving time windows of the length 3000 "samples" (300000 time cycles), taking with mutual shift = 300 "samples" (30000 cycles). Observed values of H lie in the range 0.87-0.96 with average value 0.92. So, the energy dissipation process is a self-affine fractal curve with fractal dimension $D = 2-H = 1.08$ (in two-dimensional space). The process is persistent, i.e. it has a tendency to maintain the existing position. As to using the Hurst exponent for predictive purposes this problem needs further research.

PREDICTION OF "NON-EARTHQUAKES"

The problem of predictability of SOC systems is vitally important for their applications. Theoretically, prediction time of such systems is limited by the largest positive Lyapunov exponent of the system. However, large external noise can decrease this limit. There exist several methods of prediction of chaotic non-linear systems [17], [18].

We suggest a new approach to predictability of future states of CA, namely: to try to predict the sites where a large event in the nearest future is impossible (or only small events are possible). An important question is: what information is available for prediction? If we suppose that we know the states of all sites at moment t then we can predict with probability one all those sites where no event in the next moment $(t+1)$ is possible (or, only small events are possible). Perhaps, such situation may seem unrealistic from practical point of view but it is interesting as a theoretical limit of predictability under condition of full information about the system. And besides, usual assumption that prediction should be based only on catalog of events seems to be somewhat non-justified since one has often supplementary information on the process under question furnished by other physical fields.

So, we have derived some statistics of "non-fires" under assumption of full information about the states of FF-model. The results are collected in Table 1. We see that considerable

part of time-space volume of the model (nearly 88%) can be predicted with probability one as fire-free territory for the nearest future.

We believe that any information on non-events in the future for particular sites is of some use to the problem of seismic risk assessment. Of course, under non-full information about the system states or in the case when only catalog of past events is available the special search is necessary to find precursors of non-events in the same manner as it has being done for prediction of large events. We hope to undertake such a search in the future.

DISCUSSION AND FUTURE PROBLEMS

We summarize now our preliminary experience with FF models. These models exhibit definitively many SOC features. They are very simple and have modest computer-time demands. Thus, it is easy to collect catalogs of very large sizes and to perform a thorough statistical analysis of very subtle or rare phenomena in their evolution. They can be easily modified and generalized with a view to bring them nearer to the seismicity or other natural processes.

In the present form FF models hardly can be interpreted in terms of stick-slip motion of faults or rock fracturing process. But this circumstance does not seem to be very substantial. The initial sand-pile model looked as a rather abstract CA and only later on it was modified so that now it is recognized as an adequate model for seismicity.

We would like to enumerate some future problems in studying FF models which seem to us interesting and promising.

1. Modifications of FF models and studying their properties in the context of seismicity.
   For example, we could introduce for each tree-site a variable characterizing its size and make this size to grow with time till some threshold. Further, we could introduce a stochasticity and a long-distance range of match action. Thus, the model might become more adequate to seismicity.
2. Investigation of oscillations of energy dissipation prior to large events based on wavelet analysis.
   Log-periodic oscillations (LPO) of dissipated energy (or some other parameter) were observed for different cellular automata and natural systems including seismicity, geochemical processes, acoustic emission and even stock market prices [7]-[9]. The technique for extraction LPO from data developed by Sornette et al. [7]-[9] consists in a parametric estimation with some prescribed signal form including logarithmically accelerating frequency. This parametric form is derived from an assumption of cyclic scaling (so-called Discrete Scale Invariance in dissipation process). Such assumption has no clear physical basis. That is why we suggest to use the modern wavelet analysis in order to detect a signal of arbitrary form. Further investigations will permit to estimate its statistical efficiency and possible superiority over the Sornette method.
3. The search for precursors of "non-earthquakes" and statistical estimation of their efficiency.
   Any information of "non-events" in the future for particular sites is of some use to the problem of seismic risk assessment. Of course, under non-full information about the system states or in the case when only catalog of past events is available a special search is necessary to find precursors of "non-events" in the same manner as it has being done for prediction of large events.

4. The possibilities of using the Hurst exponent ***H*** in prediction purposes.
   The Hurst exponent ***H*** has proved to be an informative parameter in many natural processes (see e.g. [16]). Especially it is useful for chaotic processes of the Brownian motion type (the energy dissipation process of FF-model behaves just in this manner). So, temporal variations of the Hurst exponent might be connected to large events.

The authors thank Prof.V.I.Keilis-Borok and Prof.D.Turcotte who had initiated this work. This publication was supported by a subcontract with Cornell University, Department of Geological Sciences under Prime Agreement No.EAR-9423818 from the National Science Foundation.

REFERENCES

1. Wiesenfeld,K.,C.Tang, and P.Bak, A Physicist's Sandbox, J.of Statist. Physics, 54, 1441-1458, 1989.
2. Burridge,R. and L.Knopoff, Model and Theoretical Seismicity, Bull.Seism. Soc.Am., 57, 341-371, 1967.
3. Carlson, J.M. and J.S.Langer, Properties of Earthquakes Generated by Fault Dynamics, Phys.Review Letters, 62, 2632-2635, 1989.
4. Main, I., Statisical Physics, Seismogenesis, and Seismic Hazard, Review of Geophysics, 34, 433-462, 1996.
5. Turcotte, D.L., Fractals and Chaos in Geology and Geophysics, 2-nd edition, Cambridge Univ. Press, New York, 1997.
6. Bak, P. and K.Chen, The Physics of Fractals, Physica D, 38, 5-12, 1989.
7. Saleur,H., C.G.Sammis, and D.Sornette, Discrete scale invariance, complex fractal dimensions, and log-periodic fluctuations in seismicity, Journ. of Geophys.Res., 101, 17,661-17, 667, 1996.
8. Johansen,A., D.Sornette, H.Wakita, U.Tsunogai, W.I.Newman, and H.Saleur, Discrete Scaling in Earthquake Precursory Phenomena: Evidence in Kobe Earthquake, Japan, J.Phys. I France, 6, 1391-1402, 1996.
9. Sornette,D., A.Johansen, and J.-P.Bouchaud, Stock Market Crashes, Precursors and Replicas, J.Phys. I France, 6, 167-175, 1996.
10. Brown,S.R., C.H.Scholz, and J.B.Rundle, A simplified spring-block model of earthquakes, Geophys.Res.Letters, 18, 215-218, 1991.
11. Brillinger D.R. Time series. Data analysis and theory. Holt, Rinehart and Winston, Inc., N.Y., Chicago, San Francisco (1975).
12. Hannan E.J. Multiple time series. John Wiley and Sons, Inc., N.Y., London, Sydney, Toronto (1970).
13. Press W.H., B.P.Flannery, S.A.Teukolsky, and W.T.Vettering, Numerical Recipes, 2-nd edition, Chapter 13, Wavelet Transforms, Cambridge Univ. Press, Cambridge, 1996.
14. Chui, C.K., An Introduction to Wavelets, Academic Press, San Diego, CA, 1992.
15. Mandelbrot,B.B. and J.R.Wallis, Noah, Joseph, and Operational Hydrology, Water Resources Research, 4, 909-918, 1968.
16. Feder, J., Fractals, Plenum Press, New York, 1988.
17. Abarbanel,H.D.I., R.Brown, and J.B.Kadtke, Prediction in chaotic non-linear systems: Methods for time series with broad band Fourier spectra, Phys.Review A, 41, 1782-1807, 1990.
18. Farmer,J.D. and J.J.Sidorovich, Predicting chaotic time series, Phys. Rev.Letters, 59, 845-848, 1987.

FIGURE CAPTIONS

Fig.1. Histogram of sizes ("energy") E in FF model, lattice 1024x32. sparkling period $T = 25$

Fig.2. Spectral peak in energy dissipation process at intermediate frequency range.

Fig.3. Frequency-time behaviour of average canonical coherence coefficient of 4 non-overlapping parts, 256x32, of FF model, 1024x32, sparkling period $T = 25$, time-window is equal to 2048.
A mean canonical coherence of amplitude about 0.4 at frequency 0.0008 is seen; this frequency corresponds to spectral peak in Fig.2a

Fig.4. Wavelet analysis of energy process prior to the largest fires in FF model, 1024x32, sparkling period $T = 25$. Daubechies wavelets of the 12-th order were used [15]; different levels (1-11) correspond to different degrees of MRA; the Level 1 characterizes the most high-frequency parts of signal wnile Level 11 characterizes one of the most smooth parts; horizontal axis is time; vertical axes give absolute values of coefficients in wavelet expansion for a given time; local maxima correspond to large coefficients; the time of largest fire in analized interval is marked by dash line; maxima in adjacent Levels are connected by poligonal line; one can discern two branches of time-moving maxima prior to the large event: descending and ascending. They can be interpreted as oscillations with decreasing frequency and with increasing frequency correspondingly. Whether the ascending branch has a linear growth of frequency with time or a log-periodic form as it follows from DSI assumption is difficult to judge now because of low signal-noise ratio. More accurate analysis will permit answer this question. The descending branch of oscillations was not observed earlier.

Fig.5. Spatio-temporal trajectory of large fires in FF model, 1024x32, sparkling period $T = 25$.
Vertical axis, X, corresponds to the larger side (1024) of rectangular model, (1024x32);
noticeable alternation of X - coordinate in time is seen

Fig.6. Time evolution of the Hurst exponent H for FF model, 1024x32, sparkling period $T = 25$, time-window is 300000 cycles.
a). deviations of energy process from a linear trend; vertical bars correspond to the largest fires;
b). evolution of the Hurst exponent in time;
energy dissipation is a self-affined fractal curve with fractal dimension $D = 2 - H = 1.08$; the process is persistent

FIGURE CAPTIONS

Fig.1. Histogram of sizes ("energy") E in FF model, lattice 1024x32. sparkling period $T = 25$

Fig.2. Power spectra of deviations of cumulative energy from a linear trend for FF models. Sparkling period $T = 25$.
a). FF model, 1024x32; spectral peak is seen at the period = 1293
b). FF model, 100x100; spectral peak is seen at the period = 400
c). CA model of spring-block type [14], 1024x32, dissipation rate is 0.23; nothing but linear behaviour is seen

Fig.3. Frequency-time behaviour of average canonical coherence coefficient of 4 non-overlapping parts, 256x32, of FF model, 1024x32, sparkling period $T = 25$, time-window is equal to 2048.
A mean canonical coherence of amplitude about 0.4 at frequency 0.0008 is seen; this frequency corresponds to spectral peak in Fig.2a

Fig.4. Wavelet analysis of energy process prior to the largest fires in FF model, 1024x32, sparkling period $T = 25$. Daubechies wavelets of the 12-th order were used [15]; different levels (1-11) correspond to different degrees of MRA; the Level 1 characterizes the most high-frequency parts of signal wnile Level 11 characterizes one of the most smooth parts; horizontal axis is time; vertical axes give absolute values of coefficients in wavelet expansion for a given time; local maxima correspond to large coefficients; the time of largest fire in analized interval is marked by dash line; maxima in adjacent Levels are connected by poligonal line; one can discern two branches of time-moving maxima prior to the large event: descending and ascending. They can be interpreted as oscillations with decreasing frequency and with increasing frequency correspondingly. Whether the ascending branch has a linear growth of frequency with time or a log-periodic form as it follows from DSI assumption is difficult to judge now because of low signal-noise ratio. More accurate analysis will permit answer this question. The descending branch of oscillations was not observed earlier.

Fig.5. Spatio-temporal trajectory of large fires in FF model, 1024x32, sparkling period $T = 25$.
Vertical axis, X, corresponds to the larger side (1024) of rectangular model, (1024x32);
noticeable alternation of X - coordinate in time is seen

Fig.6. Time evolution of the Hurst exponent H for FF model, 1024x32, sparkling period $T = 25$, time-window is 300000 cycles.
a). deviations of energy process from a linear trend; vertical bars correspond to the largest fires;
b). evolution of the Hurst exponent in time;
energy dissipation is a self-affined fractal curve with fractal dimension $D = 2 - H = 1.08$; the process is persistent

Table 1

Distribution of all possible events, which could occur at a given time moment

1-st column - Size of Event with non-zero number of FF-cluster.

2-nd column - its empirical function of distribution

3-rd column - number of different FF-clusters with such a size

Time = 3980000

0	.878946	
20882		
1	.947176	1621
2	.964012	400
3	.973861	234
4	.980428	156
5	.983416	71
6	.986194	66
7	.988214	48
8	.989604	33
9	.990740	27
10	.991624	21
11	.992297	16
12	.992718	10
13	.993350	15
14	.994149	19
15	.994402	6
16	.994781	9
17	.995328	13
18	.995581	6
19	.996001	10
20	.996380	9
21	.996591	5
22	.996717	3
23	.996970	6
25	.997096	3
26	.997180	2
27	.997306	3
28	.997475	4
29	.997517	1
30	.997685	4
31	.997769	2
32	.997938	4
35	.998064	3
36	.998106	1
37	.998148	1
38	.998232	2
40	.998275	1
41	.998401	3
42	.998443	1
43	.998485	1
44	.998569	2
45	.998611	1
46	.998695	2
47	.998822	3
48	.998906	2
49	.998948	1
54	.998990	1
55	.999074	2
59	.999116	1
61	.999158	1
63	.999200	1
64	.999242	1
68	.999285	1
70	.999327	1
79	.999369	1
81	.999411	1
89	.999453	1
99	.999537	2
100	.999579	1
114	.999705	3
129	.999790	2
133	.999832	1
156	.999874	1
212	.999916	1
216	.999958	1
251	1.00000	1

Time = 4010000

0	.877748	
20843		
1	.946433	1631
2	.963067	395
3	.973975	259
4	.979365	128
5	.983576	100
6	.985640	49
7	.987787	51
8	.989346	37
9	.990735	33
10	.991830	26
11	.992883	25
12	.993346	11
13	.994020	16
14	.994315	7
15	.994820	12
16	.995031	5
17	.995283	6
18	.995536	6
19	.995620	2
20	.995705	2
21	.995831	3
22	.995999	4
23	.996168	4
24	.996421	6
25	.996673	6
26	.996800	3
27	.996926	3
28	.997094	4
29	.997347	6
30	.997558	5
31	.997642	2
32	.997768	3
33	.997810	1
34	.997852	1
35	.998021	4
36	.998105	2
37	.998189	2
38	.998316	3
39	.998400	2
40	.998484	2
41	.998526	1
42	.998610	2
43	.998653	1
44	.998695	1
45	.998737	1
47	.998779	1
48	.998863	2
49	.998905	1
50	.998948	1
51	.999032	2
52	.999074	1
53	.999116	1
54	.999158	1
60	.999200	1
61	.999242	1
63	.999285	1
67	.999327	1
71	.999369	1
72	.999411	1
78	.999453	1
82	.999537	2
84	.999622	2
87	.999664	1
89	.999706	1
101	.999748	1
114	.999790	1
144	.999832	1
180	.999874	1
184	.999917	1
213	.999959	1
359	1.00000	1

Time = 4020000

0	.883547	
21062		
1	.950289	1591
2	.965685	367
3	.974620	213
4	.979948	127
5	.983765	91
6	.986660	69
7	.988841	52
8	.989890	25
9	.990897	24
10	.991820	22
11	.992491	16
12	.993162	16
13	.993792	15
14	.994043	6
15	.994463	10
16	.994882	10
17	.995134	6
18	.995386	6
19	.995595	5
20	.995805	5
21	.995931	3
22	.996141	5
23	.996267	3
24	.996476	5
25	.996644	4
26	.996812	4
27	.996938	3
28	.997064	3
30	.997315	6
31	.997525	5
32	.997567	1
33	.997651	2
34	.997777	3
35	.998028	6
36	.998112	2
37	.998238	3
38	.998406	4
40	.998490	2
41	.998532	1
45	.998616	2
46	.998658	1
47	.998742	2
48	.998784	1
50	.998826	1
54	.999035	5
55	.999077	1
60	.999119	1
61	.999161	1
64	.999203	1
68	.999245	1
70	.999287	1
75	.999329	1
78	.999371	1
79	.999413	1
85	.999455	1
93	.999497	1
95	.999539	1
96	.999581	1
100	.999623	1
109	.999665	1
115	.999707	1
116	.999749	1
117	.999791	1
120	.999833	1
135	.999875	1
181	.999916	1
226	.999958	1
275	1.00000	1

Time = 4040000

0	.879394	
20489		
1	.948281	1605
2	.964848	386
3	.973862	210
4	.978883	117
5	.982746	90
6	.985321	60
7	.987424	49
8	.989184	41
9	.990085	21
10	.990815	17
11	.991588	18
12	.992188	14
13	.992746	13
14	.993390	15
15	.993776	9
16	.994420	15
17	.994978	13
18	.995407	10
19	.995665	6
20	.995879	5
21	.996180	7
22	.996480	7
23	.996566	2
24	.996824	6
25	.996910	2
26	.997210	7
27	.997339	3
28	.997382	1
29	.997468	2
30	.997596	3
31	.997639	1
32	.997682	1
33	.997768	2
34	.997854	2
35	.997983	3
36	.998025	1
37	.998068	1
38	.998240	4
39	.998369	3
40	.998497	3
41	.998583	2
42	.998669	2
44	.998755	2
46	.998798	1
47	.998841	1
51	.998884	1
52	.998927	1
54	.999055	3

60	.999098	1
61	.999141	1
65	.999184	1
71	.999270	2
82	.999313	1
86	.999356	1
90	.999399	1
106	.999442	1
110	.999485	1
113	.999527	1
121	.999570	1
128	.999613	1
130	.999656	1
133	.999699	1
137	.999742	1
148	.999785	1
160	.999828	1
226	.999871	1
243	.999914	1
245	.999957	1
287	1.00000	1

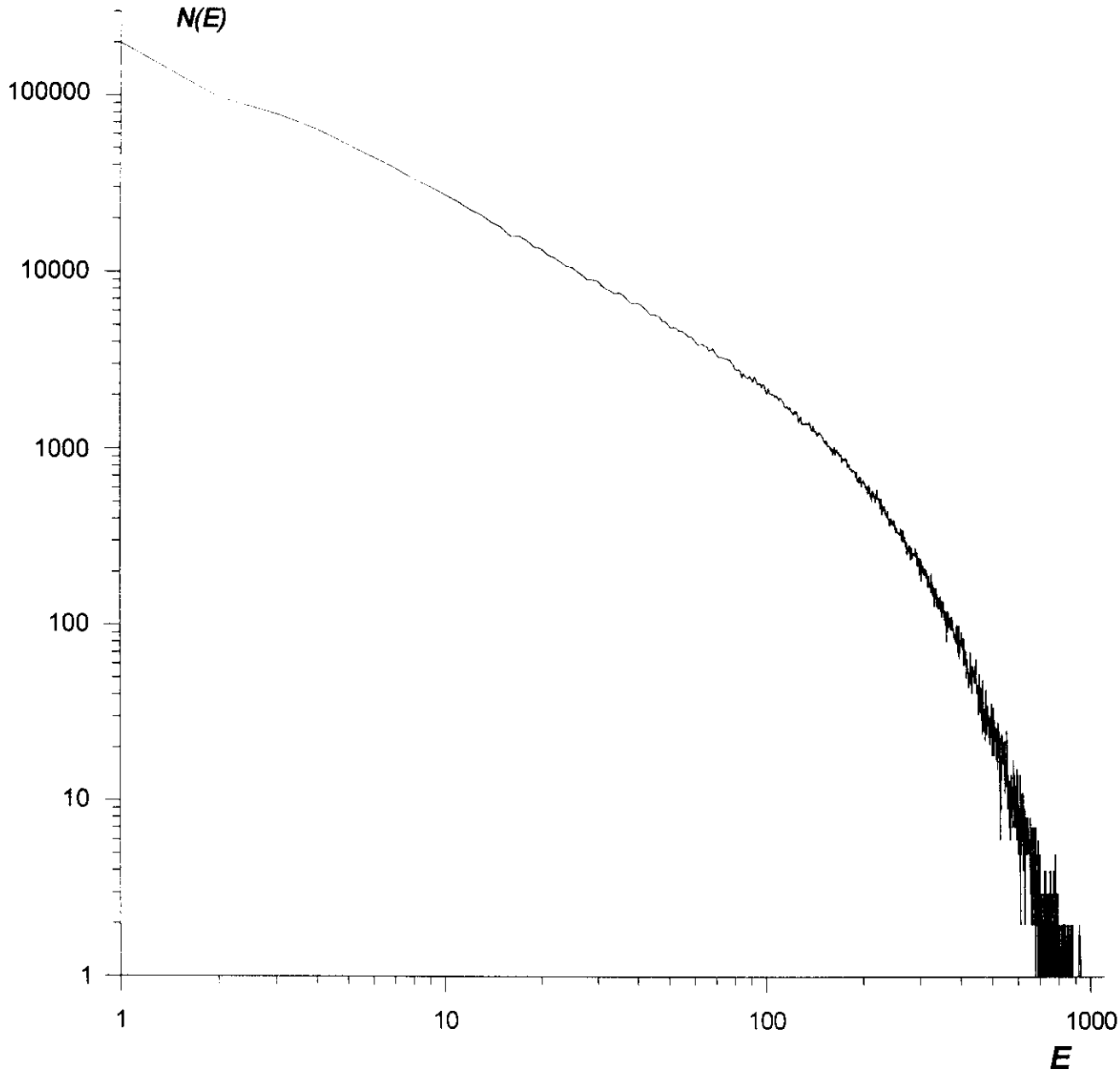

Fig.1. Histogram of sizes ("energy") E in FF model, lattice 1024x32. sparkling period T = 25

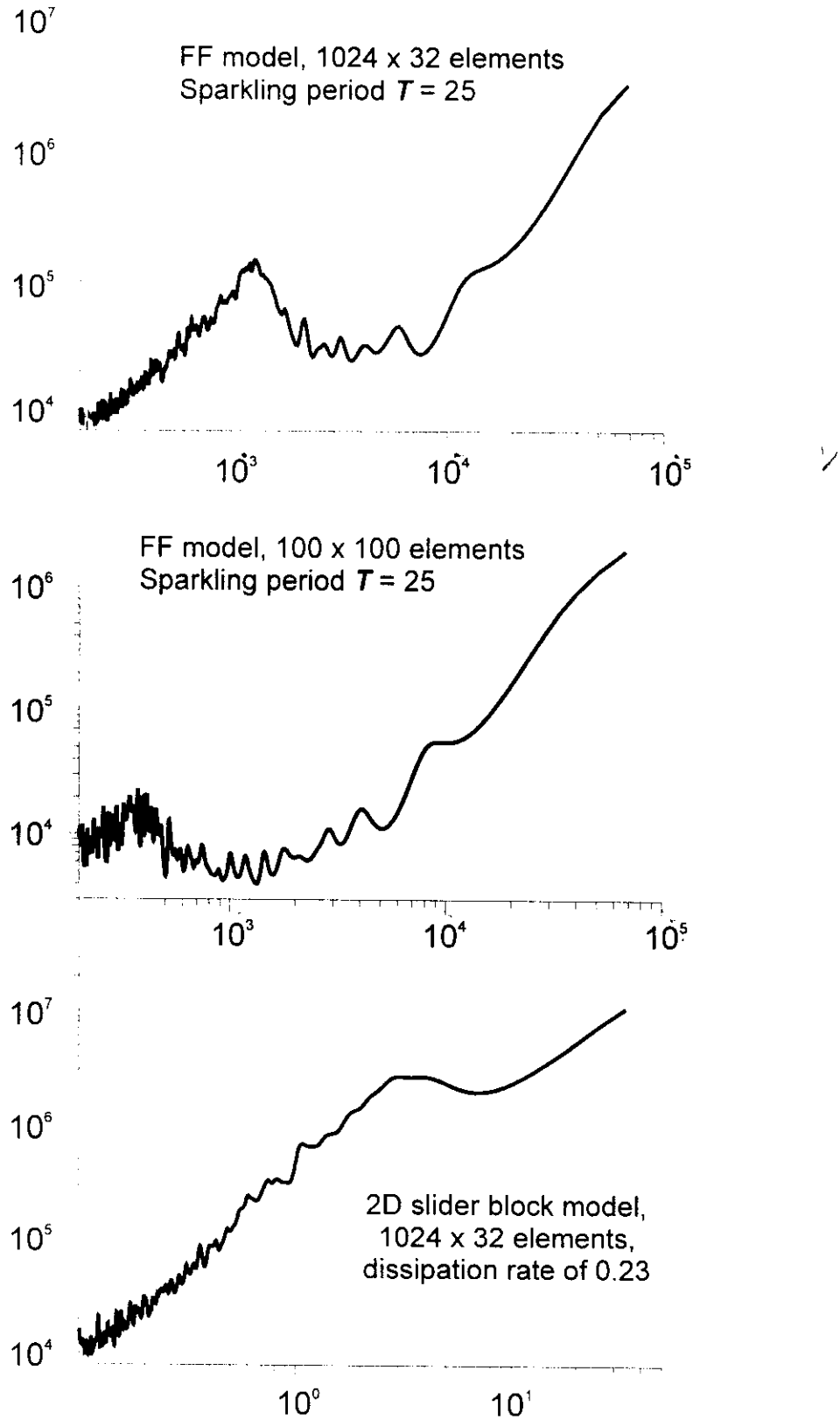

Fig. 2. Spectral peak in energy dissipation process at intermediate frequency range

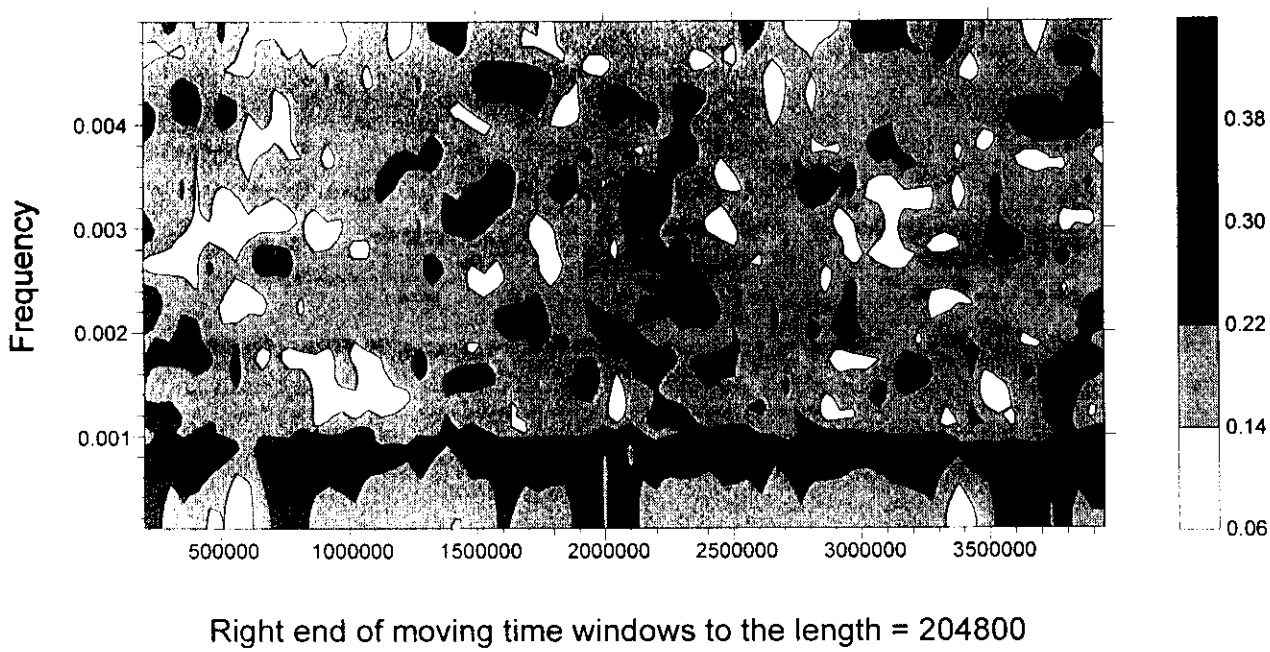

Fig. 3. Frequency-time behavior of average canonical coherence coefficient of 4 non-overlapping parts, 256x32, of FF model, 1024x32, sparkling period T=25, time-window is equal to 2048.
A mean canonical coherence of amplitude about 0.4 at frequency 0.0008 is seen; this frequency corresponds tp spectral peak in upper graph of Fig.2.

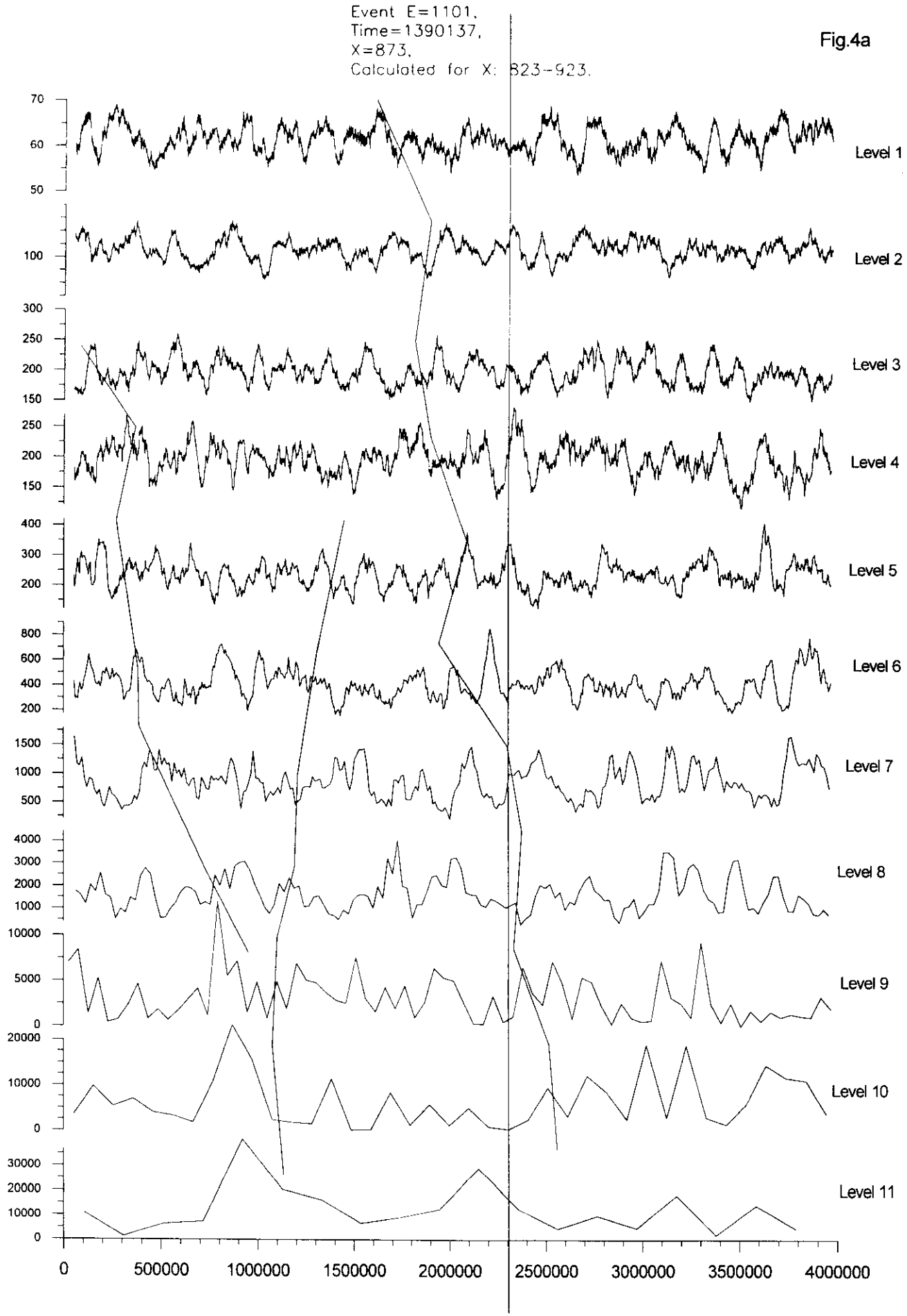
Event E=1101,
Time=1390137,
X=873,
Calculated for X: 823-923.
Level 1
Level 2
Level 3
Level 4
Level 5
Level 6
Level 7
Level 8
Level 9
Level 10
Level 11
0
500000
1000000
1500000
2000000
2500000
3000000
3500000
4000000

Fig.4a

Event E=1065,
Time=2305048,
X=645,
Calculated for X: 595-695.

Fig.4c

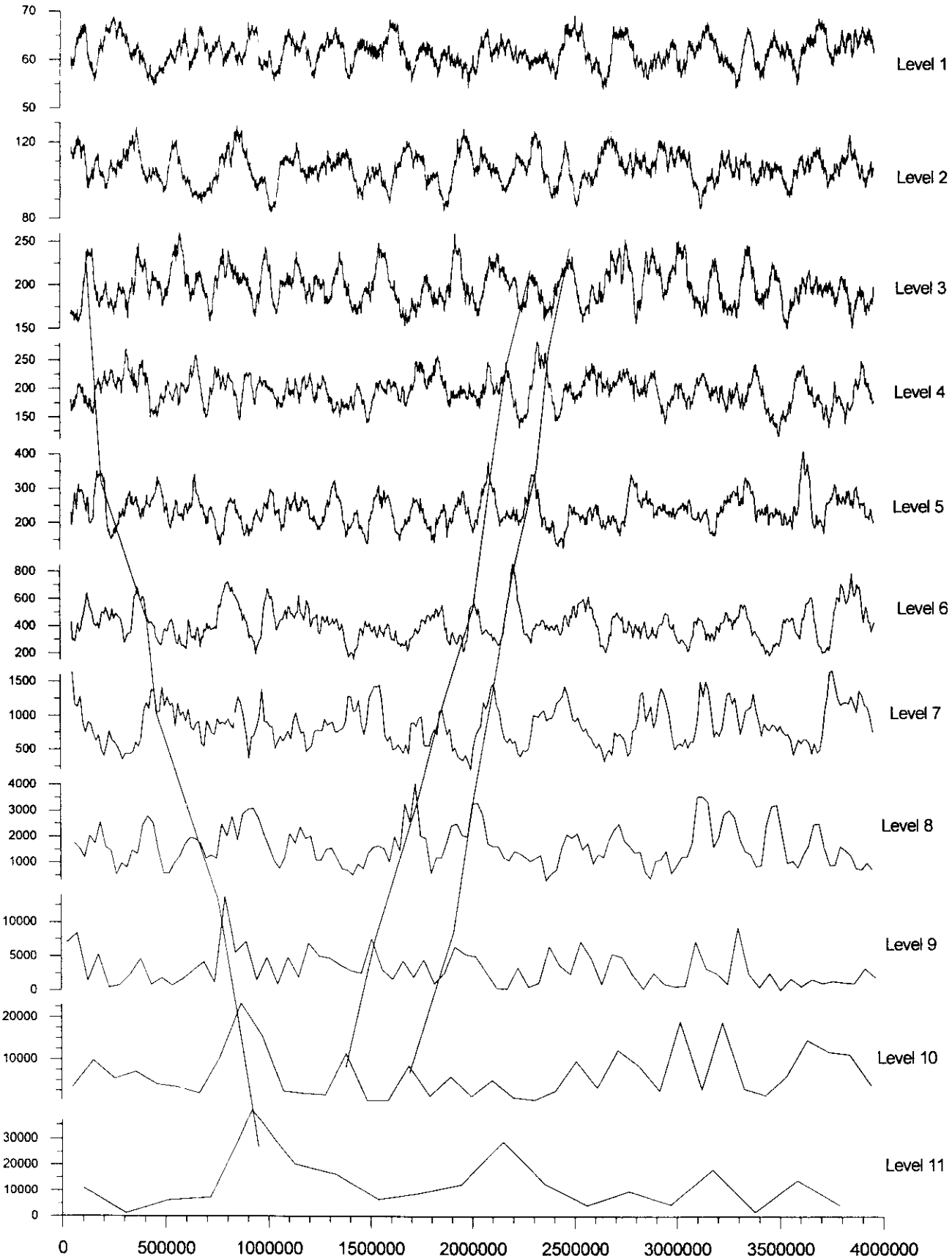

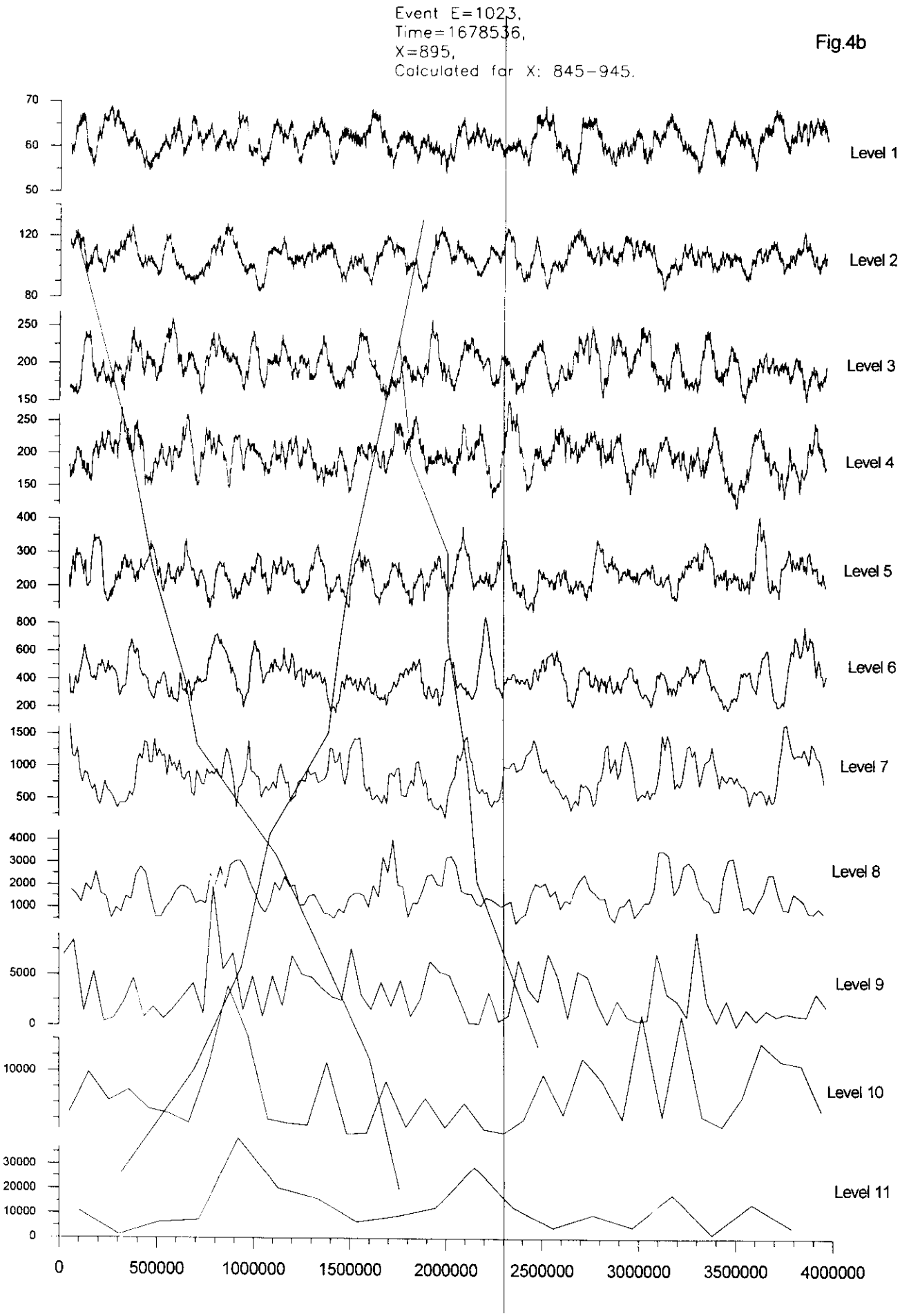
Event E=1023,
Time=1678536,
X=895,
Calculated for X: 845-945.
Level 1
Level 2
Level 3
Level 4
Level 5
Level 6
Level 7
Level 8
Level 9
Level 10
Level 11
0
500000
1000000
1500000
2000000
2500000
3000000
3500000
4000000

Fig.4b

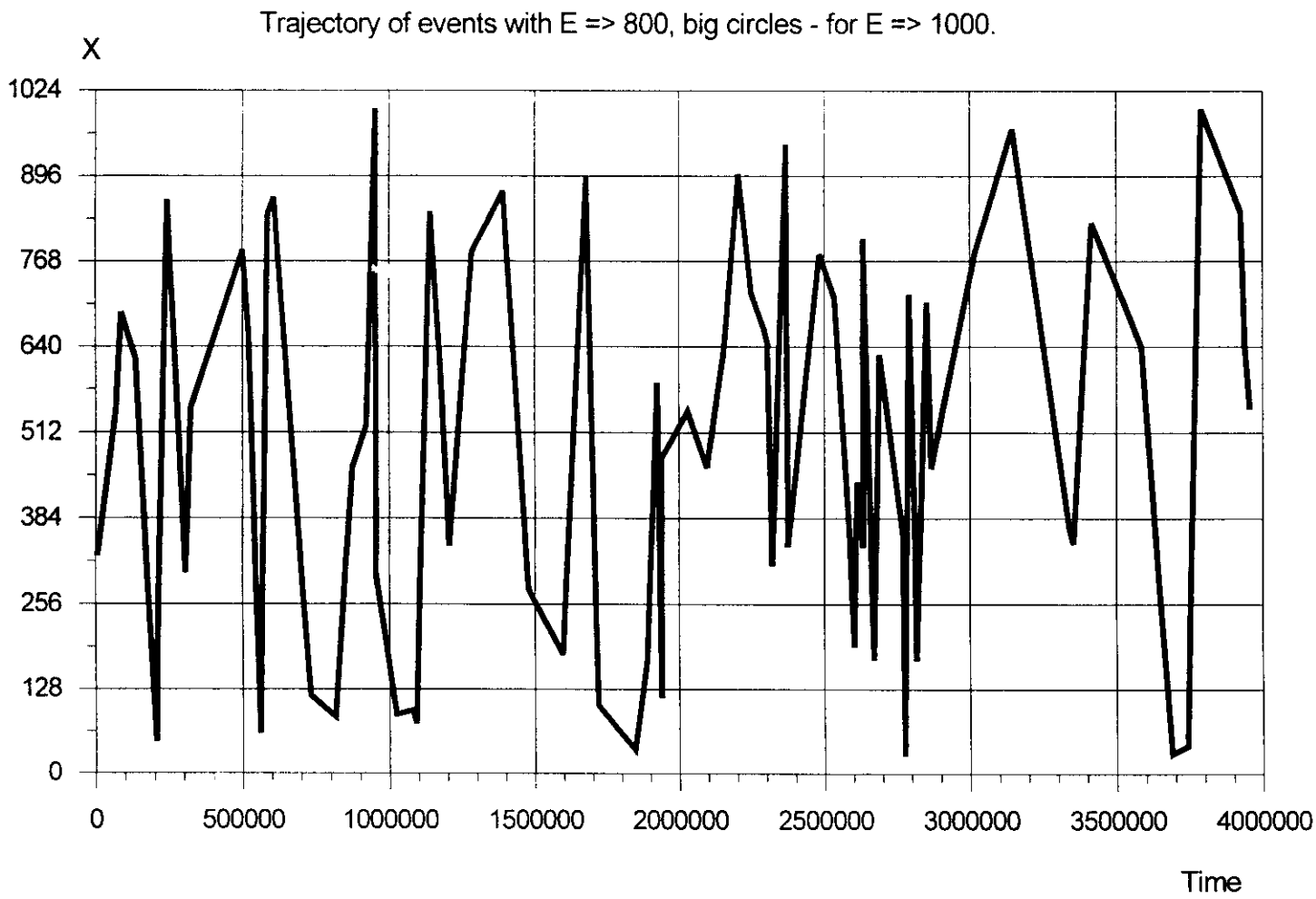

Fig.5. Spatio-temporal trajectory of large fires in FF model, 1024x32, sparkling period T = 25.
Vertical axis, X, corresponds to the larger side (1024) of rectangular model, (1024x32);
noticeable alternation of X - coordinate in time is seen

Fig.6

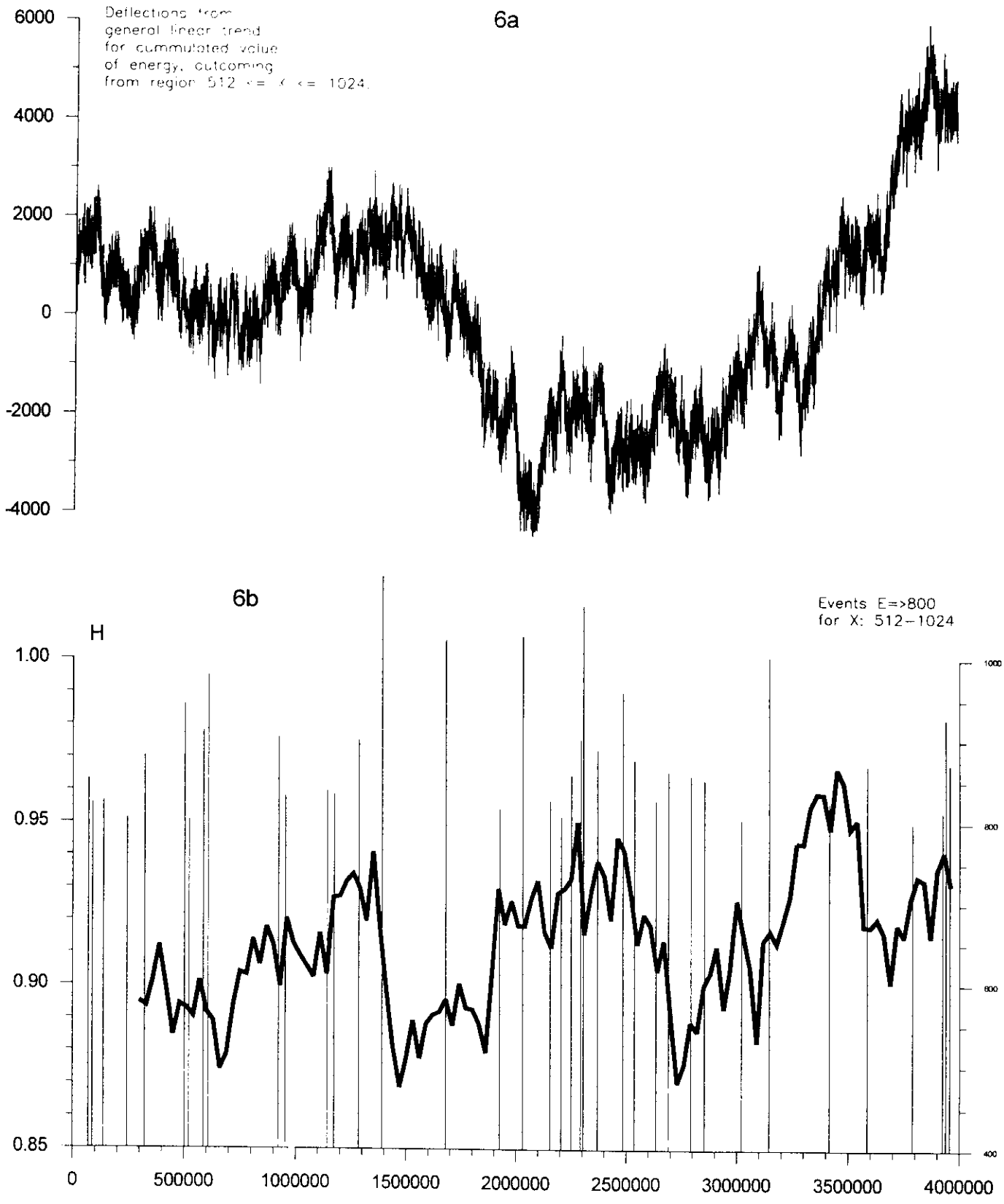
6a
Deflections from
general linear trend
for cummulated value
of energy, outcoming
from region 512 <= X <= 1024.
6000
4000
2000
0
-2000
-4000
6b
H
Events E=>800
for X: 512-1024
1.00
0.95
0.90
0.85
1000
800
600
400
0
500000
1000000
1500000
2000000
2500000
3000000
3500000
4000000